Chromogranin A regulates gut permeability *via* the antagonistic actions of its proteolytic peptides

Elke M. Muntjewerff[1*], Kechun Tang[2*], Lisanne Lutter[3,4], Gustaf Christoffersson[5,6], Mara J.T. Nicolasen[1], Hong Gao[10], Gajanan D. Katkar[7], Soumita Das[8], Martin ter Beest[1], Wei Ying[10], Pradipta Ghosh[7,9,10], Sahar El Aidy[11], Bas Oldenburg[4], Geert van den Bogaart[1,11#], Sushil K. Mahata[2,10#]

[1]Department of Tumor Immunology, Radboud Institute for Molecular Life Sciences, Radboud University Medical Center, Nijmegen, the Netherlands; [2]VA San Diego Healthcare System, 3350 La Jolla Village Drive, San Diego, CA, USA; [3]Center for Translational Immunology, Utrecht University Medical Center, Utrecht, the Netherlands; [4]Department of Gastroenterology and Hepatology, Utrecht University Medical Center, Utrecht, the Netherlands; [5]Science for Life Laboratory and [6]Department of Medical Cell biology, Uppsala University, Uppsala, Sweden; [7]Departments of Cellular and Molecular Medicine, [9]Pathology, [10]Medicine, University of California San Diego, La Jolla, CA, USA; [11]Department of Molecular Immunology and Microbiology, Groningen Biomolecular Sciences and Biotechnology Institute, University of Groningen, Groningen, the Netherlands.

*shared co-first authorship

[#]**Correspondence should be addressed to**: Sushil K. Mahata, smahata@health.ucsd.edu (ORCID: 0000-0002-9154-0787) and Geert van den Bogaart, g.van.den.bogaart@rug.nl (ORCID: 0000-0003-2180-6735).

Short title: Catestatin regulates gut permeability

Abstract

Aim: A 'leaky' gut barrier has been implicated in the initiation and progression of a multitude of diseases, e.g., inflammatory bowel disease, irritable bowel syndrome, celiac disease, and colorectal cancers. Here we show how pro-hormone Chromogranin A (CgA), produced by the enteroendocrine cells, and Catestatin (CST: $hCgA_{352-372}$), the most abundant CgA-derived proteolytic peptide, affect the gut barrier.

Methods Colon tissues from region-specific CST-knockout (CST-KO) mice, CgA-knockout (CgA-KO) and WT mice were analyzed by immunohistochemistry, ultrastructural and flowcytometry studies. FITC-dextran assays were used to measure intestinal barrier function. Mice were supplemented with CST or CgA fragment pancreastatin (PST: $CgA_{250-301}$). The microbial composition of cecum was determined. CgA and CST levels were measured in blood of IBD patients.

Results: CST-KO mice displayed (i) elongated tight, adherens junctions and desmosomes similar to IBD patients, and (ii) gut inflammation. Consistently, plasma FITC-dextran measurements showed increased intestinal paracellular permeability in the CST-knockout mice. This correlated with a higher ratio of Firmicutes to Bacteroidetes, a dysbiotic pattern commonly encountered in various diseases. Supplementation of CST-knockout mice with recombinant CST restored paracellular permeability and reversed inflammation, whereas CgA-knockout mice supplementation with CST and/or PST in CgA-KO mice showed that intestinal paracellular permeability is regulated by the antagonistic roles of these two peptides: CST reduces and PST increases permeability.

Conclusion: The pro-hormone CgA regulates the intestinal paracellular permeability. CST is both necessary and sufficient to reduce permeability and primarily acts via antagonizing the effects of PST.

Keywords

Catestatin, chromogranin A, Inflammatory bowel disease, enteroendocrine cells, epithelial tight junctions, gut barrier

Introduction

The intestinal tract harbors 10^3-10^{11} bacteria/ml [1] that in aggregate can constitute >1 g of endotoxin [2]. Endotoxins stimulate immune cells in the lamina propria, which can trigger mucosal inflammation [3]. Such inflammation can result in luminal dysbiosis [4] and gut barrier defects [5-8]. The gut barrier is comprised of a surface mucus layer which separates intact bacteria and large particulates from the mucosa [9] and the colonic epithelium which provides a physical and immunological barrier separating the body from the luminal contents (e.g., dietary antigens, a diverse intestinal microbiome, and pathogens) [10-12]. Mucosal homeostasis is maintained by the delicate and complex interactions between epithelial cells, immune cells, and luminal microbiota [10].

The gastrointestinal epithelium not only forms the body's largest interface with the external environment, but also establishes a selectively permeable epithelial barrier; it allows nutrient absorption and waste secretion while preventing the entry of luminal contents. The epithelial barrier is regulated by a series of intercellular junctions between polarized cells: an apical tight junction (TJ), which guards paracellular permeability, the subjacent adherens junction (AJ) and desmosomes; the AJs and desmosomes do not seal the paracellular space but provide essential adhesive and mechanical properties that contribute to paracellular barrier functions [11].

The permeability of the barrier is regulated by many factors such as the immune system. For example, tumor necrosis factor (TNF)-α increases the flux of larger molecules, such as proteins and other macromolecules, through the leak pathway, and interleukin (IL)-13 selectively enhances the flux of small molecules and ions via the pore pathway [5]. TNF-α plays crucial roles in the Caveolin-1-mediated internalization of Occludin (OCLN), which elevates gut permeability. Conversely, overexpression of OCLN alleviates the cytokine-induced increase in gut permeability [6]. Interferon (IFN)-γ increases gut permeability by reducing the expression of Tight junction protein ZO-1 (TJP1) and OCLN as well as by modulating actin-myosin cytoskeleton interactions with TJ proteins [7]. The simultaneous presence of TNF-α and IFN-γ deteriorates intestinal integrity by dissociating TJ proteins [8].

Here we show that the permeability of the gut barrier is regulated by the pro-hormone Chromogranin A (CgA). CgA is an acidic secretory proprotein [13] that is abundantly expressed in enteroendocrine cells (EECs) of the gut and serves as a common marker for the EECs of the gut [14]. Originally, CgA was identified as a cellular packaging factor [15-17]. However, the pro-hormone CgA is proteolytically cleaved, both intracellularly as well as extracellularly after its secretion, giving rise to seven bioactive peptides that exert a wide variety of regulatory functions among the metabolic [18-21], cardiovascular [22-25] and immune systems [26-30]. Among these bioactive peptide hormones are catestatin (CST: $hCgA_{352-372}$) [31,32] and pancreastatin (PST: $hCgA_{250-301}$) [33]. Blood plasma levels of both intact CgA [34-36] and CST [37] are increased in patients with

102 inflammatory bowel disease (IBD). We show that CST is abundantly generated in the gut.
103 Unexpectedly, we found that CgA regulates the paracellular permeability of the gut via
104 the antagonistic actions of its two peptides, PST and CST; while PST is a pro-
105 inflammatory, pro-obesigenic and anti-insulin peptide [20] which loosens the barrier, CST
106 acts as anti-inflammatory, antiobesigenic, anti-microbial, and proinsulin peptide [25,27,29]
107 that appears to be necessary and sufficient to neutralize the actions of PST and tighten
108 the barrier. Using knockout (KO) mice in conjunction with recombinant proteins, we show
109 that CST exerts its actions *via* counteracting PST.
110

Results

CgA is extensively processed to CST

To study the role of CgA and its peptides in the regulation of the gut barrier, we used systemic CgA-KO (deletion of exon 1 and ~1.5 kbp proximal promoter, thereby completely inactivating the *Chga* allele) [22] and CST-KO mice (the 63 bp CST domain of CgA was deleted from Exon VII of the *Chga* gene) [38]. CST-KO mice show low grade inflammation in the heart, pancreas, and liver and have an elevated blood pressure, are obese and suffer from insulin resistance [27,38]. We analyzed the function and morphology of the gut barrier in CST-KO mice. We used transmission electron microscopy (TEM) to resolve the ultrastructure of EECs and to evaluate the subcellular compartment where hormones are stored and released, i.e., dense core vesicles (DCVs). While DCV numbers were reduced in both CgA-KO and CST-KO mice, DCV areas were smaller in CgA-KO mice but larger in CST-KO mice (Fig. 1A&B). WT colon showed a lower concentration of CgA (average 0.019 nmol/mg protein) than of CST (average 0.37 nmol/mg protein), indicating extensive processing of CgA to CST (Fig. 1C). As anticipated, in CST-KO mice the levels of CgA in the colon were similar to that in WT mice, but those of CST were undetectable (Fig. 1C). Consistent with enhanced processing of CgA, we found increased expression of the proteolytic enzymes Cathepsin L (*Ctsl*, which cleaves CST from CgA) and Plasminogen (*Plg*, the precursor of plasmin, which is involved in CgA processing) in CST-KO and CgA-KO, respectively (Fig. 1D) [39,40].

Because the processing of CgA to CST is compromised in several diseases [41-43], we determined plasma CgA and CST levels in patients with Crohn's disease and with ulcerative colitis, both with active disease and in remission (Fig. 1E&F). In line with previous findings [34-36], we found higher CgA levels in plasma of patients with active Crohn's disease but not in patients in remission. In contrast, we found higher plasma CST levels in Crohn's disease regardless of disease activity, indicating that the processing of CgA to CST is more efficient in active disease. Patient characteristics are provided in Supplemental Table S1&S2.

CST-KO mice have a 'leaky' gut

Ultrastructural evaluation of the gut epithelium revealed that the TJs, AJs and desmosomes are significantly different in CST-KO mice compared to wild-type (WT): the TJs, AJs and desmosomes were elongated, as also observed in IBD patients (Fig. 2A, C-E, Fig. 3H-L). We determined whether this altered morphology was caused by an altered expression of proteins involved in these epithelial junctions. Gene expression studies showed a trend towards mRNA expression of multiple TJ-markers such as Occludin (*Ocln*), MARVEL domain-containing protein 2 (*Marveld2*, also called Tricellulin), Junctional adhesion molecule A (JAM-A; *F11r*) Tight junction protein ZO-1 (*Tjp1*) [44] and the desmosomal protein Desmoglein 2 (*Dsg2*), which is required for maintenance of

151 intestinal barrier function [45]. We observed concomitant elevated mRNA expression of the
152 genes coding for TJ components Claudin 1 and 2 (*Cldn1* and *Cldn2*), TJ protein ZO-2
153 and 3 (*Tjp2* and *Tjp3*), and AJ genes coding for alpha-E-Catenin (*Ctnna1*), Cadherin-
154 associated protein (*Ctnnb1*), and Cadherin 1 (*Cdh1*) (Fig. 2F&G). Primer sequences are
155 provided in Supplemental Table S3. For Occludin, ZO-1, alpha-E-Catenin, Cadherin 1,
156 Claudin 1, we did not observe significantly altered protein levels. However, we did find
157 expression at both the mRNA and protein levels of *Cldn2* (Fig. 2F, Fig. 3A&G), a specific
158 claudin that is known to increase the paracellular flux of cations and water through the
159 pore pathway [46].
160 In order to assess the functional consequence of the altered cellular junctions, we
161 determined the flux through the leak pathway, which is responsible for the paracellular
162 movement of larges molecules, including microbial proteins and other macromolecules.
163 Compared to WT mice, we observed a more than 10-fold increase in leakage of plasma
164 FITC-dextran (4 kDa) in the CST-KO mice (Fig. 2B). This confirms that the intestine in
165 CST-KO mice has a strongly diminished paracellular barrier via the leak pathway,
166 although the large magnitude of leakage might even suggest direct epithelial damage.
167
168 **CST-KO mice and IBD patients show comparable ultrastructural changes in tight**
169 **junctions, adherens junctions, and desmosomes.**
170 Ultrastructural analyses of colonic mucosa revealed increased lengths of TJ, AJ, and
171 desmosomes in IBD patients compared to healthy controls (Fig. 3H-L). Unlike CST-KO
172 mice, IBD patients displayed a decrease in AJ diameter (Fig. 3H&K).
173
174 **The leaky gut in CST-KO mice is accompanied by mucosal inflammation and**
175 **dysbiosis**
176 Because inflammation regulates the epithelial cellular junctions [5-8] and an increased gut
177 permeability is often associated with mucosal inflammation, we investigated the immune
178 cell populations in the colons of CST-KO mice by histochemical analysis (Fig. 4A-C).
179 Indeed, the colon of CST-KO mice displayed signs of mucosal inflammation, such as
180 elevated immune cell infiltration (Fig. 4D&E), increased fibrosis (Fig. 5D&E), and
181 increased apoptosis (Fig. 6A). In addition, there was increased abundance of
182 macrophages ($CD45^+11b^+Emr1^+$) and helper $CD4^+$ T cells in the colon of CST-KO mice
183 as confirmed by flow cytometry (Fig. 4F). Moreover, CST-KO mice showed increased
184 expression of the following proinflammatory genes: TNF-α (*Tnfa*), IFN-γ (*Ifng*),
185 Chemokine CXC motif ligand 1 (*Cxcl1* aka *Kc/Gro1*), Chemokine CC motif ligand 2 (*Ccl2*
186 aka *Mcp1*), Egg-like module-containing mucin-like hormone receptor 1 (*Emr1* aka *F4/80*),
187 Integrin alpha-M (*Itgam* aka *Cd11b*), and Integrin alpha-X (*Itgax* aka *Cd11c*) (Fig. 4G).
188 Increased expression of *Tnfa, Ifng, Cxcl1*, and *Ccl2* genes correlated with increased
189 protein levels (Fig. 5A). Upregulation of proinflammatory cytokines is in line with prior
190 work demonstrating a positive correlation of IFN-γ [47] and TNF-α [44] with intestinal

leakiness. The decreased expression of anti-inflammatory cytokines, such as interleukin 4 (*Il4*) and interleukin 10 (*Il10*), in CST-KO mice is also in congruence with the reported role of anti-inflammatory cytokines in gut permeability (Fig. 5C) [48]. The decreased *Il10* mRNA levels correlated with a decreased protein level of IL-10 (Fig. 5C). Furthermore, the expression of *S100a9* gene (forming Calprotectin in complex with S100a8) was increased in colon of CST-KO mice and Calprotectin protein levels were increased in plasma, colon and feces of CST-KO mice (Fig. 5B); increased Calprotectin, a protein secreted by activated neutrophils and macrophages, has been shown to be associated with increased intestinal permeability [49]. The increased inflammation in the gut of CST-KO mice is consistent with the known anti-inflammatory roles of CST [29,50] and with our previous observation of low-grade systemic inflammation in the CST-KO mice [27].

Because a leaky gut may either cause or be the consequence of altered luminal microbes [51], we investigated whether the microbial population in CST-KO mice was altered. We found that the microbiome in CST-KO mice was indeed quite different in composition than its WT littermates (Fig. 6B-E&7). Most prominently, CST-KO mice showed a higher ratio of Firmicutes to Bacteroidetes (Fig. 6C-E), which is opposite to the decreased ratio observed in WT mice intra-rectally infused with CST [52], and supports the idea that a low ratio of Firmicutes to Bacteriodetes could be beneficial to dampen intestinal inflammation [52].

That the leaky gut of CST-KO mice is inflamed and harbors dysbiotic luminal contents implies that CST is required for maintaining gut barrier integrity and preventing dysbiosis and gut inflammation. This is important because a “leaky gut” [53], dysbiosis [54], and hyperactivated immunity [55] are all well known to play a role in IBD. It is also consistent with others’ observation that administration of exogenous CST can ameliorate colitis in mice [55].

CST is sufficient to tighten the leaky gut barrier in CST-KO mice and reduce inflammation

To test whether CST is sufficient to regulate gut permeability, we supplemented CST-KO mice with recombinant CST (intraperitoneal injections of 2 μg/g body weight once daily for at least 15 days), which reversed paracellular leakiness of FITC-dextran and the associated abnormalities such as: (i) reduced plasma FITC-dextran even lower than WT level (Fig. 2B), (ii) increased mRNA expression of *Ocln*, *Marveld2*, *F11r*, *Tjp1, and Dsg2* (Fig. 2F&H), (iii) decreased mRNA expression *of Cldn1, Cldn2*, *Tjp2, Tjp3, Ctnna1*, *Ctnnb1*, and *Cdh1,* as well as increased protein expression of Claudin-2 (Fig. 2F&G, 3A&C), (iv) decreased mRNA expression of proinflammatory genes (*Tnfa*, *Ifng*, *Cxcl1, Ccl2, Emr1*, *Il12b*, *Nos2*, *Itgam*, and *Itgax)* (Fig. 4G*)*, (v) increased expression of anti-inflammatory genes (*Arg1*, *Il4*, *Tgfb1*, *Il10*, *Mrc1*, *Clec7a*, and *Clec10a*) (Fig. 5C), (vi) decreased expression of Calprotectin gene (subunit *S100a9)* and protein levels (Fig. 5B). These findings demonstrate that CST reduces intestinal inflammation, and that CST is

not only required for the integrity of the paracellular gut barrier, but is also sufficient to maintain the integrity of this barrier during homeostasis.

The paracellular permeability of the gut is intact in CgA-KO mice

Next, we carried out the gut barrier studies in CgA-KO mice, which not only lack CST, but also lack all other peptides derived from CgA. Ultrastructural studies showed no structural changes in TJ, AJ and desmosomes in CgA-KO mice compared to WT mice (Fig. 8A). To our surprise, we found that despite the absence of CST in these mice, the gut permeability for FITC-dextran was not increased (Fig. 8B); if anything, the paracellular barrier was even tighter than WT control mice. This decreased permeability was not accompanied by changes in CgA-KO mice in genes coding for components of TJ, AJ and desmosomes, except that *Ocln* and *Dsg2* gene expression were decreased in CgA-KO mice compared to WT mice (Fig. 8C). Likewise, proinflammatory gene and protein expressions were not affected in CgA-KO mice (Fig. 8D-E). In line with this, histology and EM revealed some fibrosis, but no excessive immune cell infiltration in the colon of CgA-KO mice (Fig. 5D&E). In contrast to the CST-KO mice, the CgA-KO mice even showed increased colonic expression of anti-inflammatory genes and proteins (Fig. 8F-G). The decreased colon levels of Calprotectin were also consistent with decreased gut permeability (Fig. 8H). Compared to CST-KO mice, Firmicutes and Bacteroidetes bacteria populations in CgA-KO mice were more comparable to WT mice (Fig. 7&9A).

These findings suggest that CST is not essential in the absence of CgA. Because a leaky and inflamed gut was seen in the CST-KO mice which specifically lack the proteolytic fragment of CST, but not in CgA-KO mice which lack CST and all other peptides that are generated proteolytically from CgA, these findings raised the possibility that CST may be required to antagonize the actions of some other peptide hormone that is also a product of CgA.

Gut permeability is regulated by the antagonistic effects of two CgA peptides: CST and Pancreastatin (PST)

Among the various proteolytic peptides, we hypothesized that CST could be acting to balance the impact of PST, another peptide fragment of CgA (Fig. 9B). This hypothesis was guided by prior work [43] alluding to PST's deleterious impact on the gut mucosa, causing macrophage infiltration and inflammation. To test the nature of contribution of PST and CST on the gut paracellular barrier function, we supplemented the CgA-KO mice with either CST alone (2 μg/g body weight for 15 days), or PST alone (2 μg/g body weight for 15 days), or both PST and CST co-administered at equimolar ratio for 15 days. CST alone did not change leakiness of FITC-dextran in CgA-KO mice (Fig. 9C).

By contrast, PST alone increased the leakiness in CgA-KO mice and this leakiness was markedly reduced when the CgA-KO mice received both PST and CST at equimolar

concentration (Fig. 9C). These findings indicate that PST increases the paracellular gut permeability, and that CST antagonizes this action. Together, these data lead us to propose a working model (Fig. 9D) in which the intestinal epithelial paracellular barrier is finetuned by the EECs via a major gut hormone, CgA. Our data show that CgA is proteolytically processed into two peptides, CST and PST, which tighten and loosen the gut barrier, respectively.

Discussion

The major finding in this work is the discovery of a molecular mechanism that involves a major EEC-derived gut hormone that has a balanced action on the paracellular gut barrier; two hormone derivatives of CgA, i.e., CST and PST, which either tighten or loosen the barrier, respectively. Because CgA-KO mice had unimpaired leakage of FITC-dextran, which was increased by exogenous administration of PST but not reduced by exogenous CST alone, findings also indicate that the barrier-homeostatic mechanism(s) is contained within and converge at a molecular level on the prohormone CgA and its processing into counteracting peptide hormones. These findings are important because CST is a major peptide hormone in EEC which is proteolytically produced from CgA by proprotein convertase 1 (PC1) [55], cathepsin L [56], plasmin [40] and kallikrein [57]. Its abundance in the gut suggests that the permeability of the gut barrier is regulated by CST.

CgA is unique in having peptide domains that antagonize several functions including inflammation (CST suppresses while PST promotes), obesity (CST inhibits while PST stimulates) and sensitivity to insulin (CST increases while PST diminishes) [20,27,58]. Since CgA-KO mice lack both CST and PST, and we observed increased permeability in CST-KO mice and decreased permeability in CgA-KO mice, we reasoned that these opposing phenotypes are probably caused by the lack of PST in the CgA-KO mice. Indeed, the increased permeability in PST-treated CgA-KO mice and its reversal by co-treatments of PST and CST lead us to conclude that CST promotes the epithelial paracellular barrier function by counteracting PST. Nevertheless, the baseline gut permeability in CST-KO mice was higher than in CgA-KO mice supplemented with PST. This might suggest that there are other cleavage fragments of CgA that regulate the intestinal permeability or that the effects cannot be completely reversed.

While PST exerts deleterious impact on the gut mucosa, causing macrophage infiltration and inflammation [59], we found that lack of CST caused an increased expression of proinflammatory genes and proteins and treatment of CST-KO mice with CST reversed expression of those genes and proteins. These findings are in line the anti-inflammatory roles of CST [27,29] and with the low-grade systemic inflammation present in the CST-KO mice [27,29]. Our findings are also in congruence with the existing literature which showed increased TJ permeability in presence of increased proinflammatory cytokines such as TNF-α, IL-1β, and IFN-γ [60]. A reduced gut barrier function might facilitate the leakage of microbial components such as lipopolysaccharide (LPS) and peptidoglycan (PGN) from the lumen of the gut into the tissues, where they can bind to pattern recognition receptors and activate the immune system. In turn, the increased inflammation can result in further leakage of the gut. For instance, myosin light chain kinase (MLCK) plays critical roles in cytokine-mediated TJ regulation by disrupting the interaction between TJ proteins and the actin-myosin cytoskeleton [61] leading to damage of the TJ scaffold, which is crucial for the maintenance of barrier integrity [61]. Inflammatory cytokine-induced intestinal barrier loss

318 is also believed to be due to endocytosis of TJ proteins, which also requires MLCK
319 transcription and activity at the TJ [6], although we did not observe decreased protein levels
320 of TJ proteins in the colon of CST-KO mice. In addition to the above mechanisms, TNF-
321 α suppresses TJ barrier function by decreasing expression of TJP1 protein, increasing
322 expression of Claudin-2, and activating the NF-κB pathway [62]. IL-6 also increases
323 expression of Claudin-2 [63]. In line with this, we observed elevated levels of Claudin-2 in
324 the colon of CST-KO mice.
325 In addition to these indirect effects on TJ protein expression and structure via the
326 immune system, it might also be possible that CgA and/or its cleavage products exert
327 direct effects on the epithelial cells and thereby more directly regulate the TJs. To
328 investigate this, it will be interesting to perform *in vitro* experiments, e.g., epithelial
329 monolayers in perfusion chambers co-cultured with or without immune cells [64].
330 An interesting question is how CST and PST affect the AJs and desmosomes. Not
331 only TJ components, but also desmosome and AJ components are altered in CST-KO
332 mice and these changes are reversible by administration of exogenous CST. It might be
333 possible that the AJs and/or desmosomes are part of a feedback mechanism to
334 compensate the altered TJ structure. Previously, by using Dsg2-KO mice, desmosomes
335 have been shown to regulate the intestinal barrier [45]. Moreover, Dsg2 modulates the
336 production of glial cell-derived neurotrophic factor (GDNF) in inflammatory bowel disease
337 patients [65]. Therefore, a possible scenario is that CgA-derived peptides regulate the
338 release of GDNF from enteric glial cells in the gut wall, which in turn affects the epithelial
339 junctions.
340 The present study unequivocally demonstrates that CST is a key regulator of
341 paracellular gut permeability since the absence of CST (CST-KO) is accompanied by
342 dysbiosis, increased gut permeability for FITC-dextran, increased infiltration of
343 macrophages and $CD4^+$ T cells, and higher local inflammatory gene and protein
344 expression with the substitution of CST-KO mice with CST reversing many of the above
345 abnormalities. Do gut hormones simulate the actions of CST? While Cholecystokinin
346 (CCK) decreases mucosal production of proinflammatory cytokines induced by LPS and
347 increases the expression of seal forming TJ proteins (OCLN, Claudins and JAM-A) [66],
348 Ghrelin ameliorates sepsis-induced gut barrier dysfunction by activation of vagus nerve
349 via central ghrelin receptors [53] as well as by decreasing production of TNF-α and IL-6 [67].
350 Glucagon-like peptide 1 (GLP-1) has also been shown to decrease inflammation of
351 enterocytes [68]. Vasoactive intestinal peptide, a neuropeptide found in lymphocytes [69],
352 mast cells [70], and enteric neurons of the gastrointestinal tract regulates both epithelial
353 homeostasis [71] and intestinal permeability [72]. The multitude of effects of CST on gut
354 physiology and their recapitulation by these well-investigated gut hormones establishes
355 CST as an important gastrointestinal peptide hormone.
356 CST-KO mice (loss of barrier integrity) are hypertensive and insulin-resistant on
357 normal chow diet [27,38] and CgA-KO mice (intact barrier integrity) have a normal blood

358 pressure and are supersensitive to insulin in both normal chow and on high fat diet [18,20].
359 Could metabolic endotoxemia explain the above phenotypes? Besides gastrointestinal
360 peptide hormones and neuropeptides, TJ homeostasis is altered by proinflammatory
361 cytokines, pathogenic bacteria, and pathological conditions like insulin resistance and
362 obesity. Firmicutes (e.g., *Lactobacillus*, *Clostridium*, and *Enterococcus*) and
363 Bacteroidetes (e.g., *Bacteroides*) constitute the major bacterial phyla in the gut [73].
364 Toxigenic bacteria cause diarrhea *via* increased ion permeability of the pore pathway [51],
365 but gut microbes might also affect the leak pathway. Enteric pathogenic bacteria such as
366 *Escherichia coli* and *Salmonella typhimurium* alter the intestinal epithelial TJ barrier and
367 cause intestinal inflammation [74]. LPS alters expression and localization of TJ proteins
368 such as TJP1 and OCLN [75]. Therefore, it would be interesting to study whether the
369 systemic LPS levels support the observed dysbiosis-related loss of gut barrier in the CST-
370 KO mice. Since high fat diet-induced insulin-resistant mice and patients with obesity or
371 diabetes display elevated levels of Firmicutes and Proteobacteria compared to the
372 beneficial phylum Bacteroidetes [76], it is conceivable that dysbiosis (i.e., increased
373 Firmicutes and decreased Bacteroidetes) in CST-KO mice is due to their resistance to
374 insulin. This is further supported by the fact that *Akkermansia muciniphila*, which
375 regulates intestinal barrier integrity, is less abundant in diabetic individuals [77].
376 Furthermore, the daily administration of *A. muciniphila* is known to mitigate high fat-
377 induced gut barrier dysfunction [78]. Conversely, metabolic endotoxemia, resulting from the
378 loss of barrier integrity, contributes to insulin resistance and obesity [76,79]. The intact
379 paracellular barrier function in CgA-KO mice could thus be due to their heightened
380 sensitivity to insulin.
381 Human calprotectin, a 24 kDa dimer, is formed by S100A8 and S100A9 monomers
382 and released from neutrophils and monocytes. In fact, this calprotectin complex
383 constitutes up to 60% of the soluble proteins in the cytosol of neutrophils [80] and fecal
384 calprotectin levels serve as a marker of intestinal inflammation [81,82]. Because of the
385 positive correlation between calprotectin concentration in gut lavage fluid and intestinal
386 permeability [83], calprotectin levels are also used to assess intestinal permeability.
387 Increased calprotectin levels have been reported to increase intestinal permeability [49].
388 Therefore, increased gene and protein expressions in the colon of CST-KO mice are in
389 line with the increased permeability in CST-KO mice.
390 Elevated plasma CST levels in patients suffering from Crohn's disease both in
391 disease remission and flare-up as compared to elevated precursor CgA in Crohn's
392 disease flare-ups only suggests that while CgA is generally upregulated in Crohn's
393 disease, it is only efficiently processed to CST during disease remission. Previous studies
394 revealed higher plasma CgA levels during flare-ups as compared to ulcerative colitis and
395 Crohn's disease patients in remission [34]. An open question remains how the levels of PST
396 and CST are regulated in ulcerative colitis and Crohn's disease patients. For CST our
397 findings suggest a proteolytic switch, where CgA and CST are excessively produced in

398 Crohn's disease regardless of the disease state, but CgA is converted more into the anti-
399 inflammatory CST in quiescent Crohn's disease. The gut barrier dysfunction in CST-KO
400 mice is reminiscent of active Crohn's disease, because the gut permeability provided by
401 cell-cell junctions is generally diminished in IBD patients [84]. Based on our findings, we
402 hypothesize that the higher levels of CST during Crohn's disease remision promote anti-
403 inflammatory responses and aid restoration of epithelial cellular junctions.
404
405
406

407 **Material and Methods**
408
409 **Mice**. Male wild type (WT), CST-knockout (KO) and CgA-KO mice (3 weeks old) on
410 C57BL/6 background were kept in a 12 hr dark/light cycle on normal chow diet (NCD:
411 13.5% calorie from fat; LabDiet 5001, Lab Supply, Fort Worth, TX). Experiments were
412 conducted in a blinded fashion whenever possible. For terminal procedure, mice were
413 deeply anesthetized (assessed by pinching toe response) with isoflurane followed by
414 harvesting of tissues. Euthanasia was achieved through exsanguination. For rescue
415 experiments with exogenous CST and PST, mice were injected intraperitoneally with CST
416 (2 µg/g body weight) and/or PST (2 µg/g body weight) at 9:00 AM for 2-4 weeks before
417 collecting feces or harvesting tissues. All mouse studies were approved by the UCSD and
418 Veteran Affairs San Diego Institutional Animal Care and Use Committees and conform to
419 relevant National Institutes of Health guidelines.
420
421 **Gut permeability assay.** Fluorescein isothiocyanate conjugated dextran (FITC-dextran-
422 FD4, 4 kDa; MilliporeSigma, St. Louis, MO) was administered (44 mg/100 g body weight)
423 to 8 hr fasting mice by oral gavage followed by collection of blood after 4 hr of
424 administration from the heart under deep isloflurane anesthesia [85]. Plasma concentration
425 of FITC was determined by comparison of fluorescence signals with a FITC-dextran
426 standard curve.
427
428 **Measurement of tissue cytokines, CST, CgA and calprotectin.** A portion of the colon
429 was homogenized in PBS and cytokines were measured in 20 µl of the homogenate using
430 U-PLEX mouse cytokine assay kit (Meso Scale Diagnostics, Rockville, MD) via the
431 manufacturer's protocol. Mouse EIA kits from CUSABIO (CUSABIO Technology LLC,
432 Houston, TX) were used to determine CgA (CSB-EL005344MO), CST (CSB-E17357m),
433 and calprotectin (CSB-EQ013485MO).
434
435 **Determination of CgA and CST levels in human plasma.** EDTA-plasma was collected
436 from patients with Crohn's disease (N=89) and ulcerative colitis (N=101) (Supplemental
437 table S1) and healthy controls (N=50). Intestinal inflammation was assessed by
438 colonoscopy. A flare-up was defined as histological and endoscopic disease activity,
439 whereas remission entailed absence of endoscopic inflammation and histological disease
440 activity. EDTA-plasma from healthy controls (Supplementary table S2) was obtained from
441 the Mini Donor Service at the University Medical Center Utrecht. Samples were thawed
442 and diluted 50-times with extraction buffer (PBS with 0.5% Tween and 0.05% sodium
443 azide), thoroughly vortexed followed by incubation at 4°C for 20 min on a rolling device.
444 Afterwards samples were centrifuged at 760 ×g for 20 min at 4°C and the supernatant
445 was collected for analysis. Samples were collected in compliance with the Declaration of
446 Helsinki. EDTA plasma was used to quantify CgA and CST using ELISA (CUSABIO CSB-

447 E17355h, CSB-E09153h). Informed consent was obtained, and the study was conducted
448 in accordance with the Institutional Board Review of the University Medical Center Utrecht
449 (approval number NL35053.041.11 & 11-050).
450
451 **Colon histological stains and immunohistochemistry.** Mouse colon was isolated,
452 washed in PBS and dehydrated in ethanol series, xylene and paraffin. Afterwards, the
453 tissue was embedded in paraffin, formalin fixed, and paraffin embedded (FFPE) and
454 sections of 5 µM were cut. Hematoxylin and eosin (HE) and Masson's trichrome (MT)
455 staining were performed using standard techniques. For the immunohistochemistry, the
456 tissue was heated in citrate buffer (pH 6.0, 1.0 nM citric acid) and endogenous peroxidase
457 activity was quenched with 3% H_2O_2 in methanol. Standard indirect immunoperoxidase
458 procedures were used for detection (Vectastain and SK-4800, Vector Laboratories) with
459 the antibody Rabbit-αKi-67 (1:100, Novus Biologicals), Rat-αF4/80 (1:500, Caltag
460 laboratories and slides were counterstained with Mayer's haematoxylin. Followed by
461 mounting using Quick D mounting medium. For fluorescent staining, slides were
462 incubated with Rabbit-αCASPIII antibody (1:100, ab2302, Abcam) and nuclear
463 counterstain with DAPI using Fluoromount-G (0100-01, Southern Biotech). Slides were
464 imaged using the PerkinElmer Vectra (Vectra 3.0.3; PerkinElmer, MA) at 20x
465 magnification or imaged using the Leica SP8 with a water dipping objective.
466
467 **Transmission Electron Microscopy (TEM) and morphometric analysis.** To displace
468 blood and wash tissues before fixation, mice were cannulated through the apex of the
469 heart and perfused with a Ca^{2+} and Mg^{2+} free buffer composed of DPBS and 9.46 mM
470 KCl as described [73]. Mouse and human colon fixation, embedding, sectioning and staining
471 were done as described [73]. Grids were viewed using a JEOL JEM1400-plus TEM (JEOL,
472 Peabody, MA) and photographed using a Gatan OneView digital camera with 4×4k
473 resolution (Gatan, Pleasanton, CA). Morphometric analyses of the dense core vesicles
474 were determined as described [86]. TJ length and diameter were determined by measuring
475 the lengths and perpendicular widths using the line tool in NIH ImageJ software.
476
477 **Tight junction protein analysis via immunoblotting.** Mouse colon pieces were
478 homogenized in a buffer containing phosphatase and protease inhibitors, as previously
479 described [19]. Colon lysates were subjected to SDS-PAGE and immunoblotted. Followed
480 by staining with Rabbit-αOccludin (1:1000, ab216327, Abcam, Cambridge, MA, USA),
481 Rabbit-αClaudin 1 (1:2000, ab180158, Abcam), Rabbit-αClaudin 2 (2µg/ml, 51-6100,
482 Thermo Fisher Scientific, Waltham, MA, USA), Mouse-αE-cadherin (1:500, 610182, BD
483 Biosciences, San Jose, CA, USA), Rabbit-αcatenin (1:1000, C2081, Sigma-Aldrich, St.
484 Louis, MO, USA) or Rat-αZO-1 (1:500, R26.4C, DSHB, Iowa City, Iowa, USA).
485

Flow cytometry analysis. Isolated colon cells from digested mouse colon were stained with fluorescence-tagged antibodies to detect macrophages ($CD45^+CD11b^+Emr1^+$) and helper T cells ($CD45^+CD4^+$). Data were analyzed using FlowJo.

Microbiome analysis. DNA was extracted from cecum of WT, CST-KO and CgA-KO (normal chow diet (NCD), littermates) using the Zymobiomics miniprep kit. Isolated DNA was quantified by Qubit (Thermo Fisher Scientific). DNA libraries were prepared using the Illumina Nextera XT library preparation kit. Library quantity and quality was assessed with Qubit and Tapestation (Agilent Technologies). Libraries were sequenced on Illumina HiSeq platform 2×150bp. Unassembled sequencing reads were directly analyzed by CosmosID bioinformatics platform (CosmosID) [87] for multi-kingdom microbiome analysis and profiling of antibiotic resistance and virulence genes and quantification of organism's relative abundance. This system utilizes curated genome databases and a high-performance data-mining algorithm that rapidly disambiguates hundreds of millions of metagenomic sequence reads into the discrete microorganisms engendering the particular sequences. Data mining, interpretation and comparison of taxonomic information from the metagenomic datasets were performed using Calyspo Bioinformatics software V.8.84.

Real Time PCR. Total RNA from colon tissue was isolated using RNeasy Mini Kit and reverse-transcribed using qScript cDNA synthesis kit. cDNA samples were amplified using PERFECTA SYBR FASTMIX L-ROX 1250 and analyzed on an Applied Biosystems 7500 Fast Real-Time PCR system. Primer sequences are in Supplemental table S3. All PCRs were normalized to *Rplp0*, and relative expression levels were determined by the $\Delta\Delta C_t$ method as described [24].

Statistics. Statistics were performed with PRISM 8 (version 8.4.3; San Diego, CA). Data were analyzed using either unpaired two-tailed Student's *t*-test for comparison of two groups or one-way or two-way analysis of variance for comparison of more than two groups followed by Tukey's *post hoc* test if appropriate. All data are presented as mean ± SEM and significance were assumed when $p<0.05$.

Declarations

Acknowledgements: We thank Zbigniew Mikulski (La Jolla Institute for Immunology, CA, USA) and Kiek Verrijp (Radboud University Medical Center, Netherland) for technical support with the histology and immunohistochemistry**.** This work was supported by grants from the Veterans Affairs (I01 BX003934 to SKM), the Human Frontier Science Program (HFSP; RGY0080/2018 to G.v.d.B), the Netherlands Organization for Scientific Research (NWO-ALW VIDI 864.14.001 to G.v.d.B), and European Research Council (grant

agreement No. 862137 to G.v.d.B). G.C. is supported by grants from the Swedish Research Council and the Swedish Society for Medical Research. S.E.A. is funded by is supported by a Rosalind Franklin Fellowship, co-funded by the European Union and University of Groningen, The Netherlands. E.M.M is supported by a short-term EMBO fellowship (EMBO7887).

Conflicts of interest: The authors declare no conflict of interest.

Availability of data and material: Primary data available from the corresponding authors on reasonable request.

539 **Figure legends**
540
541 **Fig. 1. CgA is efficiently processed to CST in the colon and CST levels correlate**
542 **with Crohn's disease activity. (A)** TEM micrographs (n=3) showing enteroendocrine
543 cell DCV in colon of WT, CgA-KO and CST-KO mice, **(B)** fewer DCV in CgA-KO and CST-
544 KO mice (1-way ANOVA) but enlarged DCV in CST-KO mice and smaller DCV in CgA-
545 KO mice (>500 vesicles from 30 micrographs) (Kolmogorov-Smirnov test). DCV, dense
546 core vesicles; Nuc, nucleus. **(C)** CgA protein and CST peptide levels in colon of WT and
547 CST-KO mice. CgA levels were comparable between WT and CST-KO mice. CST level
548 was markedly higher in WT mice and was undetectable in CST-KO mice (n=6; Welch's *t*
549 test). **(D)** Expression of proteolytic genes (n=7). *Ctsl* and *Plg* are differentially expressed
550 in colon of CgA-KO and CST-KO mice (n=8; 1-way ANOVA). **(E)** CgA and CST levels in
551 EDTA-plasma of healthy donors (Control) and Crohn's disease patients (N=89) in
552 remission or flare-up (2-way ANOVA). Ns, not significant; †, p<0.01; ‡, p<0.001.
553
554 **Fig. 2. Impaired epithelial paracellular barrier function in CST-KO mice. (A)** TEM
555 micrographs (n=3) showing tight junction (TJ), adherens junction (AJ), and desmosomes
556 (Des). MV, microvillus. **(B)** Increased gut permeability as measured by FITC-dextran level
557 in CST-KO compared to WT mice (n=8; Welch's *t* test). (**C-E**) Morphometrical analyses
558 (n=20-54) showing increased length and diameter of TJ **(C)**, AJ **(D)** and Des **(E)** in CST-
559 KO mice (Welch's *t* test). **(F-H)** Differential expression of genes in TJ (*Cldn1*, *Cldn2,*
560 *Cldn6, Ocln, Marveld2, F11r*, *Tjp1, Tjp2, and Tjp3*), AJ (*Ctnna1*, *Ctnnb1*, and *Cdh1*) and
561 Des (*Dsg2*) in colon of CST-KO mice compared to WT mice. Supplementation of CST-
562 KO mice with CST reversed the expression of the above genes (n=8; 2-way ANOVA or
563 Welch's *t* test). *, p<0.05; †, p<0.01; ‡, p<0.001.
564
565 **Fig. 3. Elevated levels of Claudin-2 in colon of CST-KO mice and elongated**
566 **epithelial junctions in IBD patients. (A)** Western blots and **(B)** densitometric analyses
567 of Claudin-1 **(B)**, Claudin-2 **(C)**, Occludin **(D)**, Tjp1 **(E)**, Catenin 1 **(F)**, and Cadherin 1 (**G**).
568 (**H&I**) TEM micrographs (n=3) showing tight junction (TJ), adherens junction (AJ), and
569 desmosomes (Des) in healthy control and IBD patients. Microvillus (MV). (**J-L**)
570 Morphometrical analyses (n=20-54) showing increased lengths and diameter of TJ (**J**),
571 AJ (**K**) and Des (**L**) in IBD patients. *, p<0.05; †, p<0.01; ‡, p<0.001.
572
573 **Fig. 4. Increased infiltration of immune cells in colon of CST-KO mice. (A-C)**
574 hematoxylin and eosin-stained histological micrographs of colon in WT **(A)**, CST-KO **(B)**,
575 and CgA-KO **(C)** mice. Arrows indicate immune cells. **(D)** Immunohistological
576 micrographs showing increased infiltration of Emr^+ cells in CST-KO mice. **(E)** TEM
577 micrographs (n=3) showing increased number of immune cells in colon of CST-KO mice.
578 Mϕ, macrophage; Cap, capillary; Ec, enterocytes; Gc, goblet cells; LP, lamina propria. **(F)**

579 Flow cytometry study (n=5-10) shows increased number of macrophages
580 ($CD45^+CD11b^+Emr1^+$) and T cells ($CD45^+CD4^+$) in colon of CST-KO mice (n=5-10;
581 Welch's *t* test). **(G)** Increased expression of proinflammatory genes (*Tnfa, Ifng, Cxcl1,*
582 *Ccl2, Emr1, Il12b, Nos2, Itgam*, and *Itgax*), which returned to WT levels after treatment
583 with CST (n=8; 2-way ANOVA). (n=8; 2-way ANOVA). *, p<0.05; †, p<0.01; ‡, p<0.001.
584
585 **Fig. 5. Elevated levels of pro-inflammatory proteins and fibrosis in colon of CST-**
586 **KO mice. (A)** Increased expression of proinflammatory proteins (Tnfα, Ifnγ, Cxcl1, and
587 Ccl2) in colon of CST-KO mice (n=8; 2-way ANOVA). **(B)** Increased expression of
588 proinflammatory Calprotectin gene *s100A9* in colon and Calprotectin protein in plasma,
589 colon, and feces of CST-KO mice, which were reversed upon administration of CST for
590 15 days (n=5; 1-way ANOVA). **(C)** Decreased expression of anti-inflammatory genes
591 (*Arg1, Il4, Tgfb1, Il10, Mrc1, Clec7a,* and *Clec10a*) (n=8; 2-way ANOVA), and anti-
592 inflammatory protein (Il10) (n=8; Welch's *t* test) in colon of CST-KO mice. CST treatment
593 increased expression of anti-inflammatory genes in CST-KO mice. **(D)** Masson's
594 trichrome-stained histological micrographs showing increased fibrosis in CST-KO and
595 CgA-KO colon. **(E)** TEM micrographs showing increased presence of collagen fibers in
596 CST-KO and CgA-KO mice. Coll, collagen; CV, clear cholinergic vesicles; MP, Meissner's
597 plexus; PV, dense core peptidergic vesicles. *p<0.05; **p<0.01; ***p<0.001.
598
599 **Fig. 6. Increased apoptosis and ratio of Firmicutes to Bacteriodetes in gut of CST-**
600 **KO mice. (A)** increased numbers of Caspase-3 positive apoptotic cells in colon of CST-
601 KO mice. **(B)** Principal CoordiNATE Analysis (PCoA) of microbiome data using Bray-
602 Curtis distance of species composition and abundance in individual WT (blue) and CST-
603 KO (red) mice. **(C-E)** Microbiota composition of cecum of WT and CST-KO mice for main
604 bacteria phyla **(C)** and the geni within the *Bacteriodetes* **(D)** and *Firmicutes* **(E).**
605
606 **Fig. 7. Detailed microbial composition of WT, CST-KO, and CgA-KO mice.** Graphs
607 show complete microbiota composition in cecum of WT **(A)**, CST-KO **(B)**, and CgA-KO
608 **(C)** mice. Circles from inside to outside show kingdom, phylum, class, order, family and
609 genus.
610
611 **Fig. 8. Increased epithelial paracellular barrier function and lower inflammation in**
612 **CgA-KO mice. (A)** Electron microscopy micrographs of colon of WT and CgA-KO mice.
613 TJ: tight junction. AJ: adherens junction. Des: desmosomes. **(B)** Gut permeability as
614 measured by FITC-Dextran plasma level in WT and CgA-KO mice (n=7; Welch's *t* test).
615 **(C)** Relative mRNA expression of genes in tight junction (*Cldn2*, *Ocln*, *Marveld2*, *F11r,*
616 and *Tjp1*) (n=8, 2-way ANOVA), adherens junction (*Ctnna1, Ctnnb1*, and *Cdh1*) (n=8; 2-
617 way ANOVA), and desmosome (*Dsg2*) (n=8; Welch's *t* test) in colon of WT and CgA-KO
618 mice. Comparable expression of **(D)** proinflammatory genes (*Tnfa, Ifng, Cxcl1, Ccl2,*

619 *Emr1, Itgam*, and *Itgax*), and **(E)** proinflammatory proteins (Tnfα, Ifnγ, Cxcl1, and Ccl2) in
620 colon of WT and CgA-KO mice (n=8, 2-way ANOVA). Increased expression of **(F)** anti-
621 inflammatory genes (*Arg1, Tgfb1, Clec7a, and Clec10a*) and comparable expression of
622 anti-inflammatory genes (*Il4, Il10,* and *Mrc1*), and **(G)** anti-inflammatory protein (Il10) in
623 colon of WT and CgA-KO mice (n=8; 2-way ANOVA or Welch's *t* test). **(H)** Comparable
624 expression of *s100a9* gene and decreased expression of calprotectin protein in CgA-KO
625 colon (n=5; Welch's *t* test). †, P<0.01; ‡, P<0.001.
626
627 **Fig. 9. Altered microbiome composition in CgA-KO mice and CST and PST**
628 **oppositely regulate gut permeability. (A)** Microbiota composition of cecum of WT and
629 CgA-KO mice for main bacteria phyla and the geni within the Bacteriodetes and
630 Firmicutes. **(B)** Scheme of CgA indicating the positions of the peptide products vasostatin
631 1, PST, CST and serpinin. **(C)** Gut permeability as measured by FITC-Dextran plasma
632 levels in WT, CST-KO and CgA-KO mice treated with saline or CST (n=8; 2-way ANOVA)
633 and in CgA-KO mice treated with PST or a combination of PST and CST (n=8; 1-way
634 ANOVA). **(D)** Model of gut barrier regulation by CST and PST. ‡, P<0.001.
635
636
637

638 **References**

639

640 1. Sender R, Fuchs S, Milo R. Revised Estimates for the Number of Human and
641 Bacteria Cells in the Body. *PLoS Biol.* 2016;14(8):e1002533.
642 2. Wassenaar TM, Zimmermann K. Lipopolysaccharides in Food, Food
643 Supplements, and Probiotics: Should We be Worried? *Eur J Microbiol Immunol*
644 *(Bp).* 2018;8(3):63-69.
645 3. Perez-Reytor D, Jana V, Pavez L, Navarrete P, Garcia K. Accessory Toxins of
646 Vibrio Pathogens and Their Role in Epithelial Disruption During Infection. *Front*
647 *Microbiol.* 2018;9:2248.
648 4. Sartor RB, Wu GD. Roles for Intestinal Bacteria, Viruses, and Fungi in
649 Pathogenesis of Inflammatory Bowel Diseases and Therapeutic Approaches.
650 *Gastroenterology.* 2017;152(2):327-339 e324.
651 5. Weber CR, Raleigh DR, Su L, et al. Epithelial myosin light chain kinase activation
652 induces mucosal interleukin-13 expression to alter tight junction ion selectivity. *J*
653 *Biol Chem.* 2010;285(16):12037-12046.
654 6. Marchiando AM, Shen L, Graham WV, et al. Caveolin-1-dependent occludin
655 endocytosis is required for TNF-induced tight junction regulation in vivo. *J Cell Biol.*
656 2010;189(1):111-126.
657 7. Scharl M, Paul G, Barrett KE, McCole DF. AMP-activated protein kinase mediates
658 the interferon-gamma-induced decrease in intestinal epithelial barrier function. *J*
659 *Biol Chem.* 2009;284(41):27952-27963.
660 8. Ye D, Ma I, Ma TY. Molecular mechanism of tumor necrosis factor-alpha
661 modulation of intestinal epithelial tight junction barrier. *Am J Physiol Gastrointest*
662 *Liver Physiol.* 2006;290(3):G496-504.
663 9. Meyer-Hoffert U, Hornef MW, Henriques-Normark B, et al. Secreted enteric
664 antimicrobial activity localises to the mucus surface layer. *Gut.* 2008;57(6):764-
665 771.
666 10. Chakaroun RM, Massier L, Kovacs P. Gut Microbiome, Intestinal Permeability, and
667 Tissue Bacteria in Metabolic Disease: Perpetrators or Bystanders? *Nutrients.*
668 2020;12(4).
669 11. Buckley A, Turner JR. Cell Biology of Tight Junction Barrier Regulation and
670 Mucosal Disease. *Cold Spring Harb Perspect Biol.* 2018;10(1).
671 12. Lutter L, Hoytema van Konijnenburg DP, Brand EC, Oldenburg B, van Wijk F. The
672 elusive case of human intraepithelial T cells in gut homeostasis and inflammation.
673 *Nat Rev Gastroenterol Hepatol.* 2018;15(10):637-649.
674 13. Winkler H, Fischer-Colbrie R. The chromogranins A and B: the first 25 years and
675 future perspectives. *Neuroscience.* 1992;49(3):497-528.
676 14. El-Salhy M, Patcharatrakul T, Hatlebakk JG, Hausken T, Gilja OH, Gonlachanvit
677 S. Chromogranin A cell density in the large intestine of Asian and European
678 patients with irritable bowel syndrome. *Scand J Gastroenterol.* 2017;52(6-7):691-
679 697.
680 15. Videen JS, Mezger MS, Chang YM, O'Connor DT. Calcium and catecholamine
681 interactions with adrenal chromogranins. Comparison of driving forces in binding
682 and aggregation. *J Biol Chem.* 1992;267(5):3066-3073.

683 16. Taupenot L, Harper KL, Mahapatra NR, Parmer RJ, Mahata SK, O'Connor DT.
684 Identification of a novel sorting determinant for the regulated pathway in the
685 secretory protein chromogranin A. *J Cell Sci.* 2002;115(Pt 24):4827-4841.
686 17. Borges R, Diaz-Vera J, Dominguez N, Arnau MR, Machado JD. Chromogranins
687 as regulators of exocytosis. *J Neurochem.* 2010;114(2):335-343.
688 18. Gayen JR, Saberi M, Schenk S, et al. A novel pathway of insulin sensitivity in
689 chromogranin a null mice: A crucial role for pancreastatin in glucose homeostasis.
690 *J Biol Chem.* 2009;284:28498-28509.
691 19. Bandyopadhyay GK, Vu CU, Gentile S, et al. Catestatin (chromogranin A(352-
692 372)) and novel effects on mobilization of fat from adipose tissue through
693 regulation of adrenergic and leptin signaling. *J Biol Chem.* 2012;287(27):23141-
694 23151.
695 20. Bandyopadhyay GK, Lu M, Avolio E, et al. Pancreastatin-dependent inflammatory
696 signaling mediates obesity-induced insulin resistance. *Diabetes.* 2015;64(1):104-
697 116.
698 21. Bandyopadhyay GK, Mahata SK. Chromogranin A Regulation of Obesity and
699 Peripheral Insulin Sensitivity. *Front Endocrinol (Lausanne).* 2017;8:20.
700 22. Mahapatra NR, O'Connor DT, Vaingankar SM, et al. Hypertension from targeted
701 ablation of chromogranin A can be rescued by the human ortholog. *J Clin Invest.*
702 2005;115(7):1942-1952.
703 23. Biswas N, Gayen J, Mahata M, Su Y, Mahata SK, O'Connor DT. Novel peptide
704 isomer strategy for stable inhibition of catecholamine release: application to
705 hypertension. *Hypertension.* 2012;60(6):1552-1559.
706 24. Mahata SK, Kiranmayi M, Mahapatra NR. Catestatin: A Master Regulator of
707 Cardiovascular Functions. *Curr Med Chem.* 2018;25(11):1352-1374.
708 25. Mahata SK, Corti A. Chromogranin A and its fragments in cardiovascular,
709 immunometabolic, and cancer regulation. *Ann N Y Acad Sci.* 2019;1455(1):34-58.
710 26. Rabbi MF, Labis B, Metz-Boutigue MH, Bernstein CN, Ghia JE. Catestatin
711 decreases macrophage function in two mouse models of experimental colitis.
712 *Biochem Pharmacol.* 2014;89(3):386-398.
713 27. Ying W, Mahata S, Bandyopadhyay GK, et al. Catestatin Inhibits Obesity-Induced
714 Macrophage Infiltration and Inflammation in the Liver and Suppresses Hepatic
715 Glucose Production, Leading to Improved Insulin Sensitivity. *Diabetes.*
716 2018;67(5):841-848.
717 28. Eissa N, Hussein H, Hendy GN, Bernstein CN, Ghia JE. Chromogranin-A and its
718 derived peptides and their pharmacological effects during intestinal inflammation.
719 *Biochem Pharmacol.* 2018;152:315-326.
720 29. Kojima M, Ozawa N, Mori Y, et al. Catestatin Prevents Macrophage-Driven
721 Atherosclerosis but Not Arterial Injury-Induced Neointimal Hyperplasia. *Thromb*
722 *Haemost.* 2018;118(1):182-194.
723 30. Muntjewerff EM, Dunkel G, Nicolasen MJT, Mahata SK, van den Bogaart G.
724 Catestatin as a Target for Treatment of Inflammatory Diseases. *Front Immunol.*
725 2018;9:2199.
726 31. Mahata SK, O'Connor DT, Mahata M, et al. Novel autocrine feedback control of
727 catecholamine release. A discrete chromogranin a fragment is a noncompetitive
728 nicotinic cholinergic antagonist. *J Clin Invest.* 1997;100(6):1623-1633.

729 32. Mahata SK, Mahata M, Fung MM, O'Connor DT. Catestatin: a multifunctional
730 peptide from chromogranin A. *Regul Pept.* 2010;162(1-3):33-43.
731 33. Tatemoto K, Efendic S, Mutt V, Makk G, Feistner GJ, Barchas JD. Pancreastatin,
732 a novel pancreatic peptide that inhibits insulin secretion. *Nature.*
733 1986;324(6096):476-478.
734 34. Zissimopoulos A, Vradelis S, Konialis M, et al. Chromogranin A as a biomarker of
735 disease activity and biologic therapy in inflammatory bowel disease: a prospective
736 observational study. *Scand J Gastroenterol.* 2014;49(8):942-949.
737 35. Sciola V, Massironi S, Conte D, et al. Plasma chromogranin a in patients with
738 inflammatory bowel disease. *Inflamm Bowel Dis.* 2009;15(6):867-871.
739 36. Wagner M, Stridsberg M, Peterson CG, Sangfelt P, Lampinen M, Carlson M.
740 Increased fecal levels of chromogranin A, chromogranin B, and secretoneurin in
741 collagenous colitis. *Inflammation.* 2013;36(4):855-861.
742 37. Zivkovic PM, Matetic A, Tadin Hadjina I, et al. Serum Catestatin Levels and Arterial
743 Stiffness Parameters Are Increased in Patients with Inflammatory Bowel Disease.
744 *J Clin Med.* 2020;9(3).
745 38. Ying W, Tang K, Avolio E, et al. The immunosuppression of macropahges
746 underlies the cardioprotective effects of catestatin (CST). *BioRxiv.* 2020.
747 39. Jiang Q, Taupenot L, Mahata SK, et al. Proteolytic cleavage of chromogranin A
748 (CgA) by plasmin: selective liberation of a specific bioactive CgA fragment that
749 regulates catecholamine release. *J Biol Chem.* 2001;276:25022-25029.
750 40. Biswas N, Rodriguez-Flores JL, Courel M, et al. Cathepsin L Co-Localizes with
751 Chromogranin a in Chromaffin Vesicles to Generate Active Peptides.
752 *Endocrinology.* 2009;150(8):3547-3557.
753 41. O'Connor DT, Kailasam MT, Kennedy BP, Ziegler MG, Yanaihara N, Parmer RJ.
754 Early decline in the catecholamine release-inhibitory peptide catestatin in humans
755 at genetic risk of hypertension. *J Hypertens.* 2002;20:1335-1345.
756 42. Chen Y, Wang X, Yang C, et al. Decreased circulating catestatin levels are
757 associated with coronary artery disease: The emerging anti-inflammatory role.
758 *Atherosclerosis.* 2019;281:78-88.
759 43. Ottesen AH, Carlson CR, Louch WE, et al. Glycosylated Chromogranin A in Heart
760 Failure: Implications for Processing and Cardiomyocyte Calcium Homeostasis.
761 *Circ Heart Fail.* 2017;10(2).
762 44. Ma TY, Iwamoto GK, Hoa NT, et al. TNF-alpha-induced increase in intestinal
763 epithelial tight junction permeability requires NF-kappa B activation. *Am J Physiol*
764 *Gastrointest Liver Physiol.* 2004;286(3):G367-376.
765 45. Gross A, Pack LAP, Schacht GM, et al. Desmoglein 2, but not desmocollin 2,
766 protects intestinal epithelia from injury. *Mucosal Immunol.* 2018;11(6):1630-1639.
767 46. Heiskala M, Peterson PA, Yang Y. The roles of claudin superfamily proteins in
768 paracellular transport. *Traffic.* 2001;2(2):93-98.
769 47. Adams RB, Planchon SM, Roche JK. IFN-gamma modulation of epithelial barrier
770 function. Time course, reversibility, and site of cytokine binding. *J Immunol.*
771 1993;150(6):2356-2363.
772 48. Howe KL, Reardon C, Wang A, Nazli A, McKay DM. Transforming growth factor-
773 beta regulation of epithelial tight junction proteins enhances barrier function and

774 blocks enterohemorrhagic Escherichia coli O157:H7-induced increased
775 permeability. *Am J Pathol.* 2005;167(6):1587-1597.
776 49. Zhernakova A, Kurilshikov A, Bonder MJ, et al. Population-based metagenomics
777 analysis reveals markers for gut microbiome composition and diversity. *Science.*
778 2016;352(6285):565-569.
779 50. Costa F, Mumolo MG, Ceccarelli L, et al. Calprotectin is a stronger predictive
780 marker of relapse in ulcerative colitis than in Crohn's disease. *Gut.* 2005;54(3):364-
781 368.
782 51. Eichner M, Protze J, Piontek A, Krause G, Piontek J. Targeting and alteration of
783 tight junctions by bacteria and their virulence factors such as Clostridium
784 perfringens enterotoxin. *Pflugers Arch.* 2017;469(1):77-90.
785 52. Rabbi MF, Munyaka PM, Eissa N, Metz-Boutigue MH, Khafipour E, Ghia JE.
786 Human Catestatin Alters Gut Microbiota Composition in Mice. *Front Microbiol.*
787 2016;7:2151.
788 53. Michielan A, D'Inca R. Host-microbiome interaction in Crohn's disease: A familiar
789 or familial issue? *World J Gastrointest Pathophysiol.* 2015;6(4):159-168.
790 54. Packey CD, Sartor RB. Commensal bacteria, traditional and opportunistic
791 pathogens, dysbiosis and bacterial killing in inflammatory bowel diseases. *Curr*
792 *Opin Infect Dis.* 2009;22(3):292-301.
793 55. Rabbi MF, Eissa N, Munyaka PM, et al. Reactivation of Intestinal Inflammation Is
794 Suppressed by Catestatin in a Murine Model of Colitis via M1 Macrophages and
795 Not the Gut Microbiota. *Front Immunol.* 2017;8:985.
796 56. Lee JC, Taylor CV, Gaucher SP, et al. Primary sequence characterization of
797 catestatin intermediates and peptides defines proteolytic cleavage sites utilized for
798 converting chromogranin a into active catestatin secreted from neuroendocrine
799 chromaffin cells. *Biochemistry.* 2003;42(23):6938-6946.
800 57. Benyamin B, Maihofer AX, Schork AJ, et al. Identification of novel loci affecting
801 circulating chromogranins and related peptides. *Hum Mol Genet.* 2017;26(1):233-
802 242.
803 58. Dasgupta A, Bandyopadhyay GK, Ray I, et al. Catestatin improves insulin
804 sensitivity by attenuating endoplasmic reticulum stress: In vivo and in silico
805 validation. *Comput Struct Biotechnol J.* 2020;18:464-481.
806 59. Eissa N, Elgazzar O, Hussein H, Hendy GN, Bernstein CN, Ghia JE. Pancreastatin
807 Reduces Alternatively Activated Macrophages, Disrupts the Epithelial
808 Homeostasis and Aggravates Colonic Inflammation. A Descriptive Analysis.
809 *Biomedicines.* 2021;9(2).
810 60. Al-Sadi R, Ye D, Dokladny K, Ma TY. Mechanism of IL-1beta-induced increase in
811 intestinal epithelial tight junction permeability. *J Immunol.* 2008;180(8):5653-5661.
812 61. Su L, Nalle SC, Shen L, et al. TNFR2 activates MLCK-dependent tight junction
813 dysregulation to cause apoptosis-mediated barrier loss and experimental colitis.
814 *Gastroenterology.* 2013;145(2):407-415.
815 62. Mankertz J, Amasheh M, Krug SM, et al. TNFalpha up-regulates claudin-2
816 expression in epithelial HT-29/B6 cells via phosphatidylinositol-3-kinase signaling.
817 *Cell Tissue Res.* 2009;336(1):67-77.

818 63. Suzuki T, Yoshinaga N, Tanabe S. Interleukin-6 (IL-6) regulates claudin-2
819 expression and tight junction permeability in intestinal epithelium. *J Biol Chem.*
820 2011;286(36):31263-31271.
821 64. van der Post S, Jabbar KS, Birchenough G, et al. Structural weakening of the
822 colonic mucus barrier is an early event in ulcerative colitis pathogenesis. *Gut.*
823 2019;68(12):2142-2151.
824 65. Schlegel N, Boerner K, Waschke J. Targeting desmosomal adhesion and
825 signalling for intestinal barrier stabilization in inflammatory bowel diseases-
826 Lessons from experimental models and patients. *Acta Physiol (Oxf).*
827 2021;231(1):e13492.
828 66. Saia RS, Ribeiro AB, Giusti H. Cholecystokinin Modulates the Mucosal
829 Inflammatory Response and Prevents the Lipopolysaccharide-Induced Intestinal
830 Epithelial Barrier Dysfunction. *Shock.* 2020;53(2):242-251.
831 67. Wu R, Dong W, Cui X, et al. Ghrelin down-regulates proinflammatory cytokines in
832 sepsis through activation of the vagus nerve. *Ann Surg.* 2007;245(3):480-486.
833 68. Drucker DJ, Habener JF, Holst JJ. Discovery, characterization, and clinical
834 development of the glucagon-like peptides. *J Clin Invest.* 2017;127(12):4217-
835 4227.
836 69. Ottaway CA, Lewis DL, Asa SL. Vasoactive intestinal peptide-containing nerves in
837 Peyer's patches. *Brain Behav Immun.* 1987;1(2):148-158.
838 70. Keita AV, Carlsson AH, Cigehn M, Ericson AC, McKay DM, Soderholm JD.
839 Vasoactive intestinal polypeptide regulates barrier function via mast cells in human
840 intestinal follicle-associated epithelium and during stress in rats.
841 *Neurogastroenterol Motil.* 2013;25(6):e406-417.
842 71. Izu LT, McCulle SL, Ferreri-Jacobia MT, Devor DC, Duffey ME. Vasoactive
843 intestinal peptide-stimulated Cl- secretion: activation of cAMP-dependent K+
844 channels. *J Membr Biol.* 2002;186(3):145-157.
845 72. Conlin VS, Wu X, Nguyen C, et al. Vasoactive intestinal peptide ameliorates
846 intestinal barrier disruption associated with Citrobacter rodentium-induced colitis.
847 *Am J Physiol Gastrointest Liver Physiol.* 2009;297(4):G735-750.
848 73. Dethlefsen L, McFall-Ngai M, Relman DA. An ecological and evolutionary
849 perspective on human-microbe mutualism and disease. *Nature.*
850 2007;449(7164):811-818.
851 74. Lemichez E, Lecuit M, Nassif X, Bourdoulous S. Breaking the wall: targeting of the
852 endothelium by pathogenic bacteria. *Nat Rev Microbiol.* 2010;8(2):93-104.
853 75. Chin AC, Flynn AN, Fedwick JP, Buret AG. The role of caspase-3 in
854 lipopolysaccharide-mediated disruption of intestinal epithelial tight junctions. *Can*
855 *J Physiol Pharmacol.* 2006;84(10):1043-1050.
856 76. Cani PD, Amar J, Iglesias MA, et al. Metabolic endotoxemia initiates obesity and
857 insulin resistance. *Diabetes.* 2007;56(7):1761-1772.
858 77. Dao MC, Everard A, Aron-Wisnewsky J, et al. Akkermansia muciniphila and
859 improved metabolic health during a dietary intervention in obesity: relationship with
860 gut microbiome richness and ecology. *Gut.* 2016;65(3):426-436.
861 78. Everard A, Belzer C, Geurts L, et al. Cross-talk between Akkermansia muciniphila
862 and intestinal epithelium controls diet-induced obesity. *Proc Natl Acad Sci U S A.*
863 2013;110(22):9066-9071.

79. Moreira AP, Texeira TF, Ferreira AB, Peluzio Mdo C, Alfenas Rde C. Influence of a high-fat diet on gut microbiota, intestinal permeability and metabolic endotoxaemia. *Br J Nutr.* 2012;108(5):801-809.
80. Johne B, Fagerhol MK, Lyberg T, et al. Functional and clinical aspects of the myelomonocyte protein calprotectin. *Mol Pathol.* 1997;50(3):113-123.
81. Mulak A, Koszewicz M, Panek-Jeziorna M, Koziorowska-Gawron E, Budrewicz S. Fecal Calprotectin as a Marker of the Gut Immune System Activation Is Elevated in Parkinson's Disease. *Front Neurosci.* 2019;13:992.
82. von Martels JZH, Bourgonje AR, Harmsen HJM, Faber KN, Dijkstra G. Assessing intestinal permeability in Crohn's disease patients using orally administered 52Cr-EDTA. *PLoS One.* 2019;14(2):e0211973.
83. Berstad A, Arslan G, Folvik G. Relationship between intestinal permeability and calprotectin concentration in gut lavage fluid. *Scand J Gastroenterol.* 2000;35(1):64-69.
84. Turpin W, Lee SH, Raygoza Garay JA, et al. Increased Intestinal Permeability is Associated with Later Development of Crohn's Disease. *Gastroenterology.* 2020.
85. Woting A, Blaut M. Small Intestinal Permeability and Gut-Transit Time Determined with Low and High Molecular Weight Fluorescein Isothiocyanate-Dextrans in C3H Mice. *Nutrients.* 2018;10(6).
86. Pasqua T, Mahata S, Bandyopadhyay GK, et al. Impact of Chromogranin A deficiency on catecholamine storage, catecholamine granule morphology and chromaffin cell energy metabolism in vivo. *Cell Tissue Res.* 2016;363(3):693-712.
87. Lax S, Smith DP, Hampton-Marcell J, et al. Longitudinal analysis of microbial interaction between humans and the indoor environment. *Science.* 2014;345(6200):1048-1052.

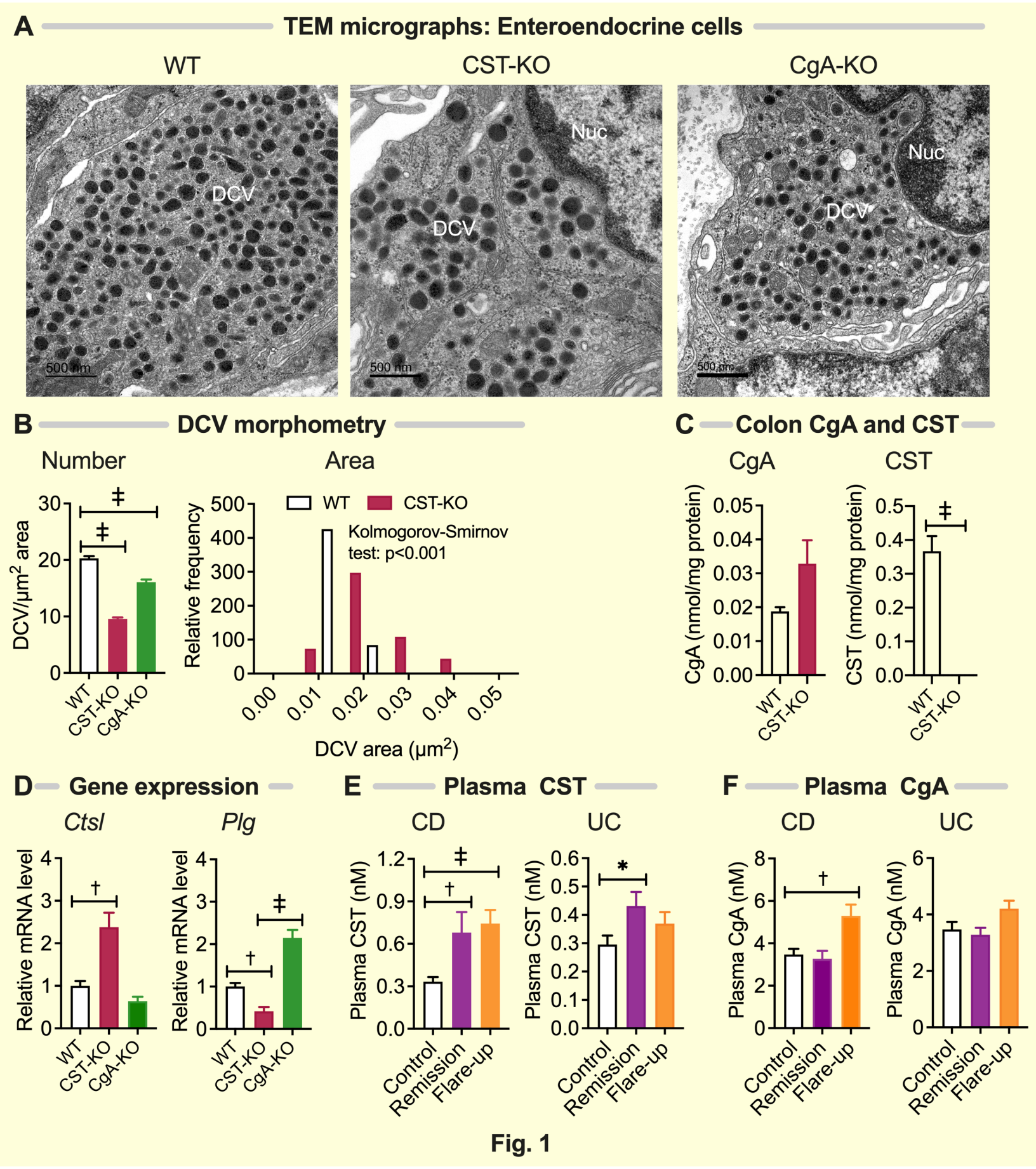
A
TEM micrographs: Enteroendocrine cells
WT
CST-KO
CgA-KO
DCV
Nuc
500 nm
B
DCV morphometry
Number
Area
DCV/μm² area
WT
CST-KO
CgA-KO
Relative frequency
Kolmogorov-Smirnov test: p<0.001
DCV area (μm²)
C
Colon CgA and CST
CgA
CST
CgA (nmol/mg protein)
CST (nmol/mg protein)
D
Gene expression
Ctsl
Plg
Relative mRNA level
E
Plasma CST
CD
UC
Plasma CST (nM)
Control
Remission
Flare-up
F
Plasma CgA
Plasma CgA (nM)

Fig. 1

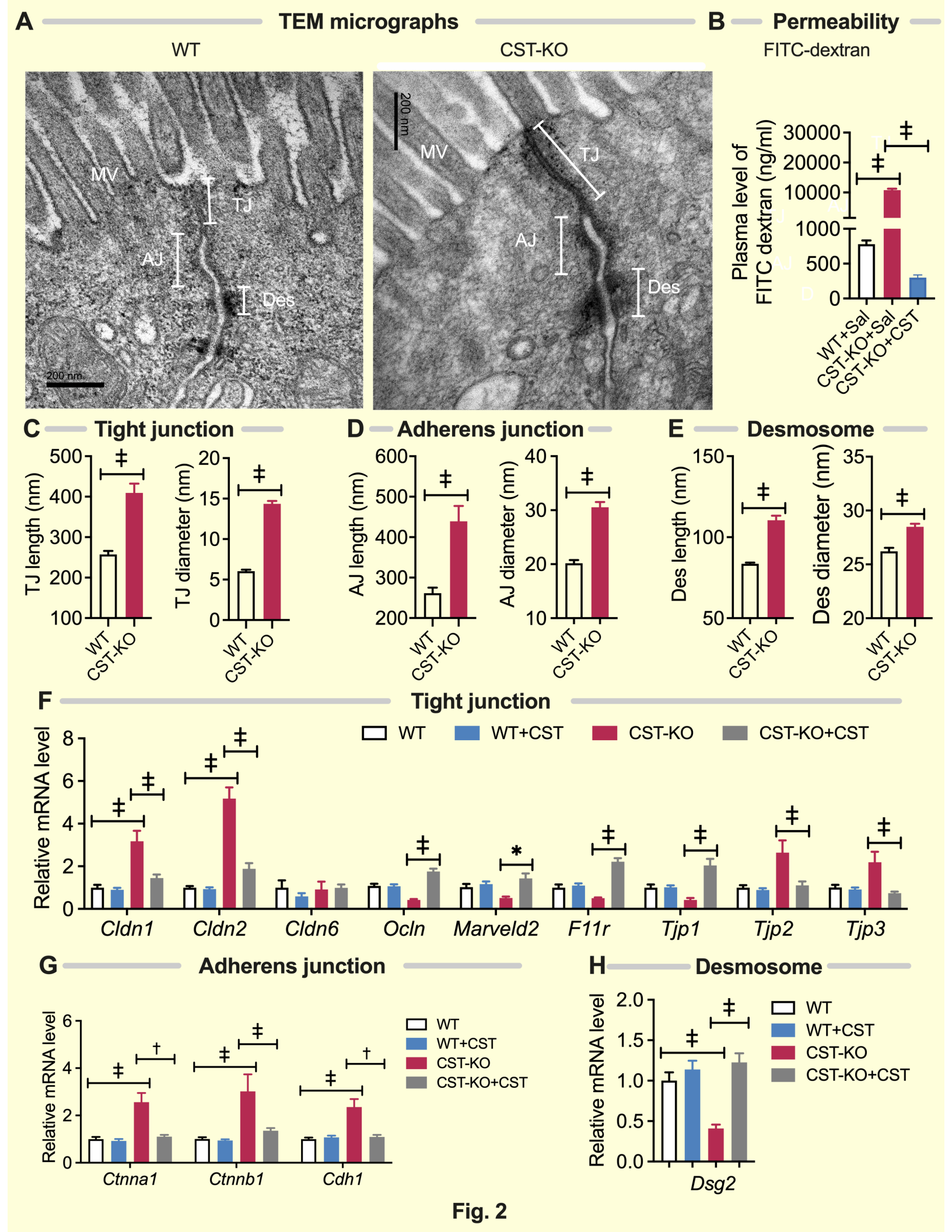
A
TEM micrographs
WT
CST-KO
MV
TJ
AJ
Des
200 nm
B
Permeability
FITC-dextran
Plasma level of FITC dextran (ng/ml)
WT+Sal
CST-KO+Sal
CST-KO+CST
C
Tight junction
TJ length (nm)
TJ diameter (nm)
D
Adherens junction
AJ length (nm)
AJ diameter (nm)
E
Desmosome
Des length (nm)
Des diameter (nm)
WT
CST-KO
F
Tight junction
WT
WT+CST
CST-KO
CST-KO+CST
Relative mRNA level
Cldn1
Cldn2
Cldn6
Ocln
Marveld2
F11r
Tjp1
Tjp2
Tjp3
G
Adherens junction
Ctnna1
Ctnnb1
Cdh1
H
Desmosome
Dsg2

Fig. 2

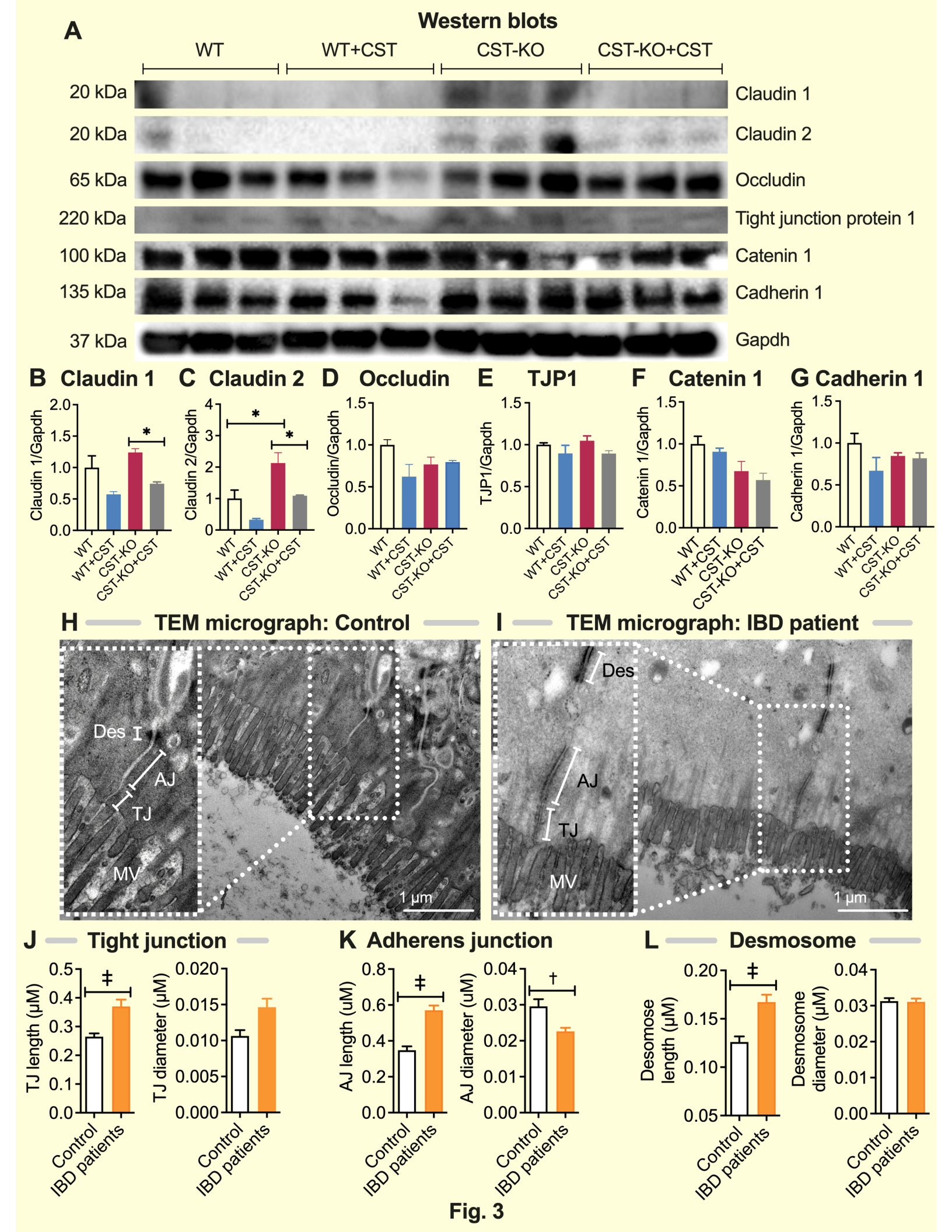
A
Western blots
WT
WT+CST
CST-KO
CST-KO+CST
20 kDa
Claudin 1
20 kDa
Claudin 2
65 kDa
Occludin
220 kDa
Tight junction protein 1
100 kDa
Catenin 1
135 kDa
Cadherin 1
37 kDa
Gapdh
B Claudin 1
Claudin 1/Gapdh
C Claudin 2
Claudin 2/Gapdh
D Occludin
Occludin/Gapdh
E TJP1
TJP1/Gapdh
F Catenin 1
Catenin 1/Gapdh
G Cadherin 1
Cadherin 1/Gapdh
H TEM micrograph: Control
Des
AJ
TJ
MV
1 µm
I TEM micrograph: IBD patient
Des
AJ
TJ
MV
1 µm
J Tight junction
TJ length (µM)
TJ diameter (µM)
K Adherens junction
AJ length (uM)
AJ diameter (uM)
L Desmosome
Desmosome length (µM)
Desmosome diameter (µM)
Control
IBD patients

Fig. 3

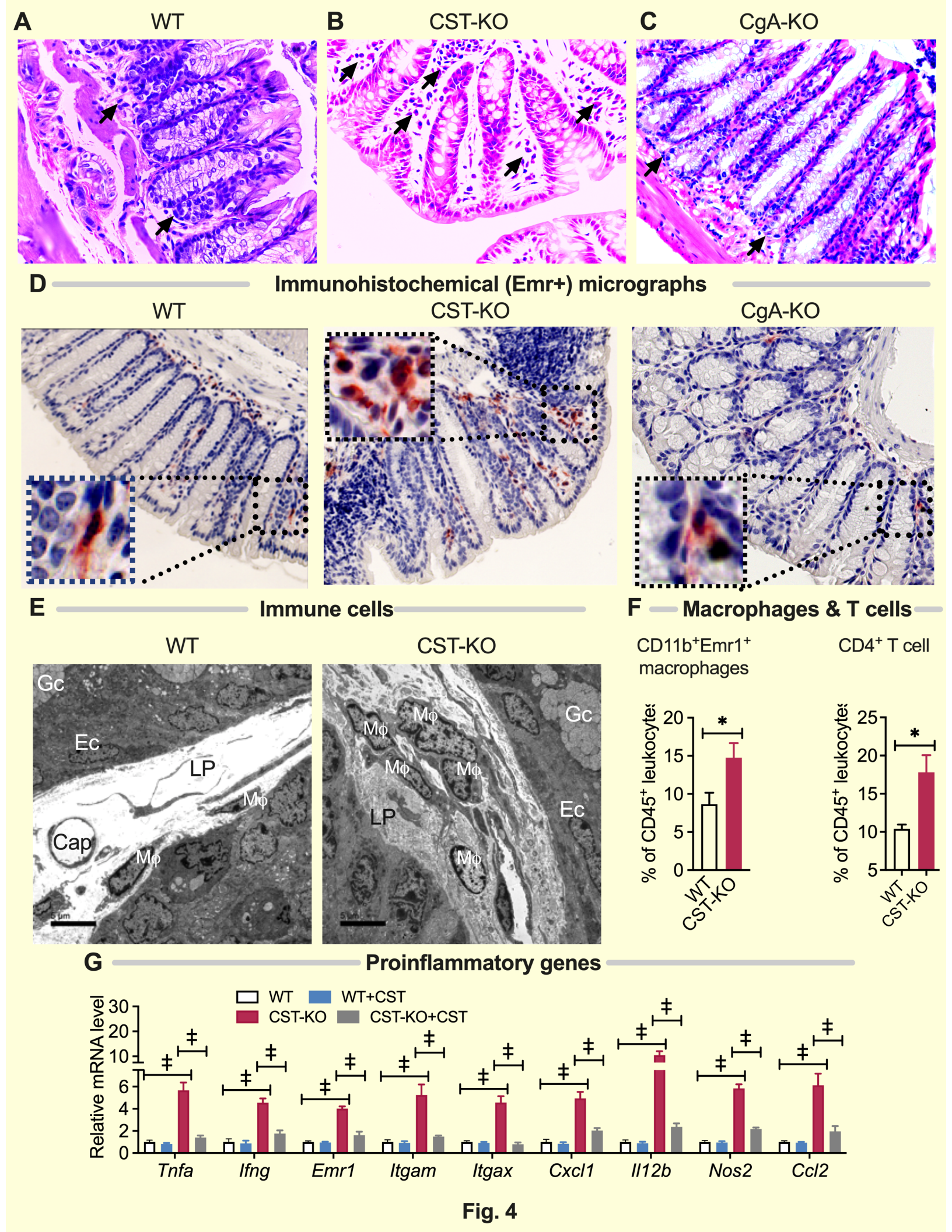
A
WT
B
CST-KO
C
CgA-KO
D
Immunohistochemical (Emr+) micrographs
WT
CST-KO
CgA-KO
E
Immune cells
WT
CST-KO
Gc
Ec
LP
Mϕ
Cap
Mϕ
Mϕ
Mϕ
Mϕ
Mϕ
Gc
LP
Ec
Mϕ
F
Macrophages & T cells
CD11b+Emr1+ macrophages
CD4+ T cell
% of CD45+ leukocytes
20
15
10
5
0
*
WT
CST-KO
% of CD45+ leukocytes
25
20
15
10
5
*
WT
CST-KO
G
Proinflammatory genes
WT
WT+CST
CST-KO
CST-KO+CST
Relative mRNA level
30
20
10
6
4
2
0
‡
Tnfa
Ifng
Emr1
Itgam
Itgax
Cxcl1
Il12b
Nos2
Ccl2

Fig. 4

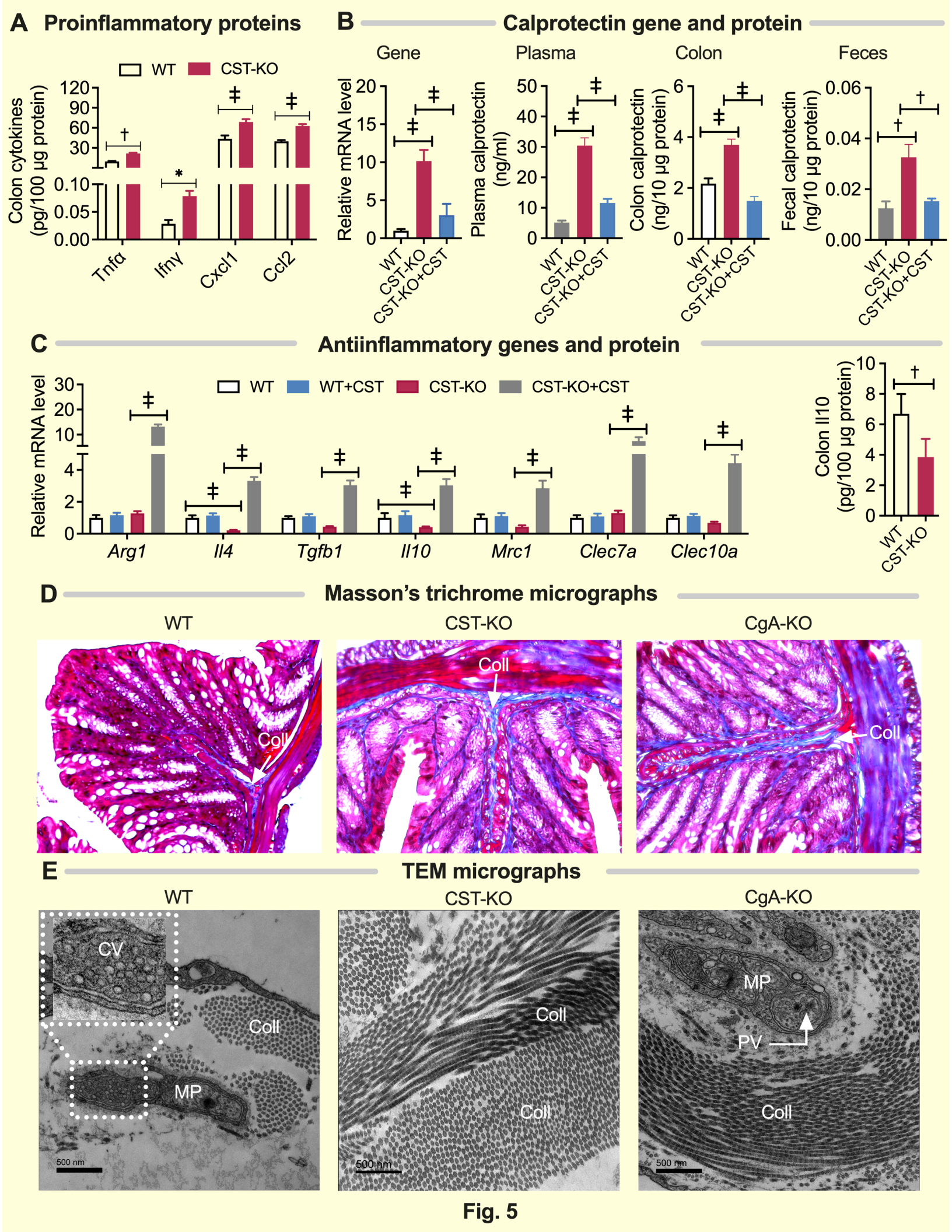
A Proinflammatory proteins
WT
CST-KO
Colon cytokines (pg/100 µg protein)
Tnfα
Ifnγ
Cxcl1
Ccl2
B Calprotectin gene and protein
Gene
Plasma
Colon
Feces
Relative mRNA level
Plasma calprotectin (ng/ml)
Colon calprotectin (ng/10 µg protein)
Fecal calprotectin (ng/10 µg protein)
WT
CST-KO
CST-KO+CST
C Antiinflammatory genes and protein
WT
WT+CST
CST-KO
CST-KO+CST
Relative mRNA level
Arg1
Il4
Tgfb1
Il10
Mrc1
Clec7a
Clec10a
Colon Il10 (pg/100 µg protein)
D Masson's trichrome micrographs
WT
CST-KO
CgA-KO
Coll
E TEM micrographs
WT
CST-KO
CgA-KO
CV
Coll
MP
PV
500 nm

Fig. 5

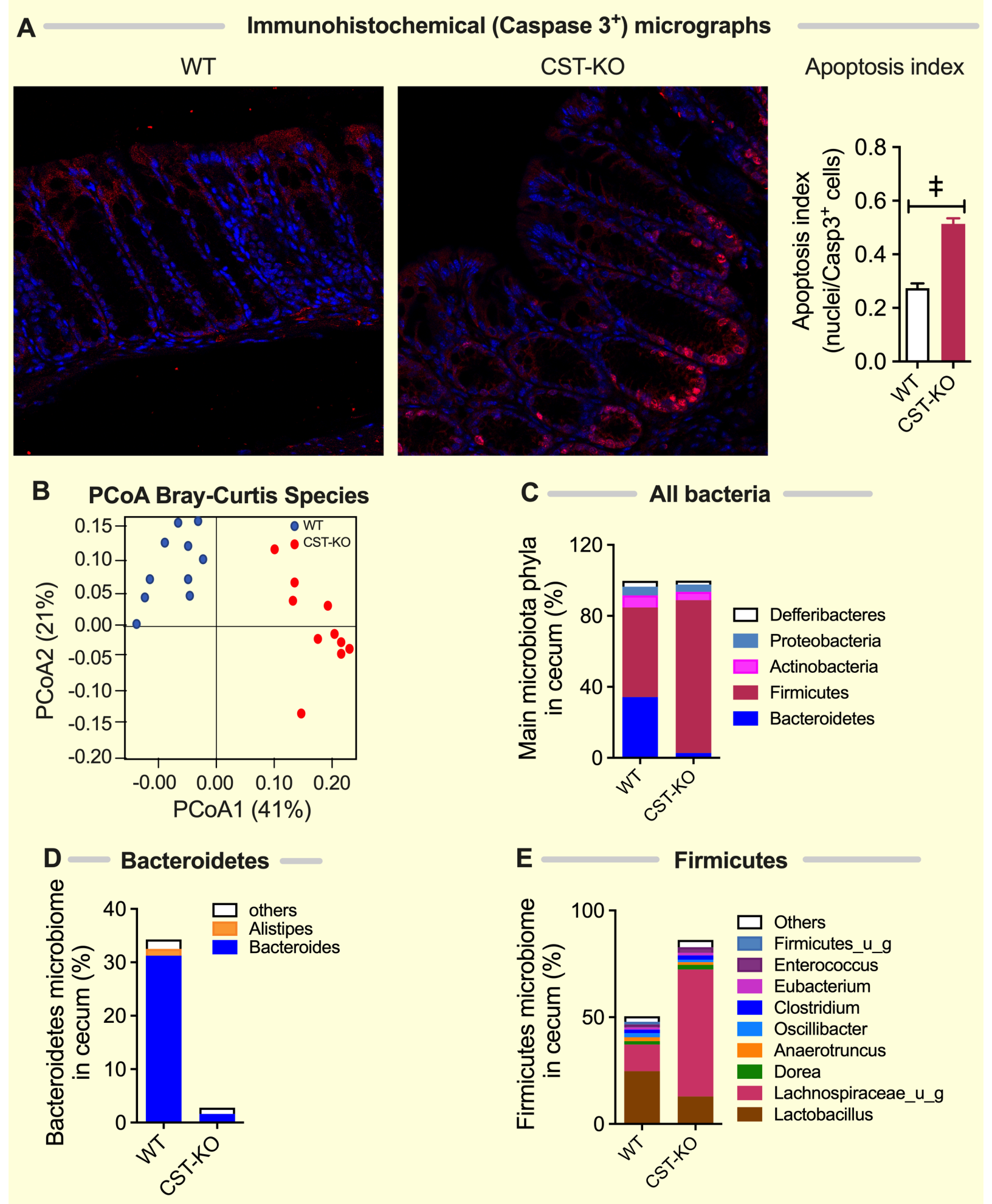
A
Immunohistochemical (Caspase 3+) micrographs
WT
CST-KO
Apoptosis index
Apoptosis index (nuclei/Casp3+ cells)
0.8
0.6
0.4
0.2
0.0
‡
WT
CST-KO
B
PCoA Bray-Curtis Species
WT
CST-KO
PCoA2 (21%)
0.15
0.10
0.05
0.00
-0.05
-0.10
-0.15
-0.20
-0.00
0.00
0.10
0.20
PCoA1 (41%)
C
All bacteria
Main microbiota phyla in cecum (%)
120
80
40
0
WT
CST-KO
Defferibacteres
Proteobacteria
Actinobacteria
Firmicutes
Bacteroidetes
D
Bacteroidetes
Bacteroidetes microbiome in cecum (%)
40
30
20
10
0
WT
CST-KO
others
Alistipes
Bacteroides
E
Firmicutes
Firmicutes microbiome in cecum (%)
100
50
0
WT
CST-KO
Others
Firmicutes_u_g
Enterococcus
Eubacterium
Clostridium
Oscillibacter
Anaerotruncus
Dorea
Lachnospiraceae_u_g
Lactobacillus

Fig. 6

A WT

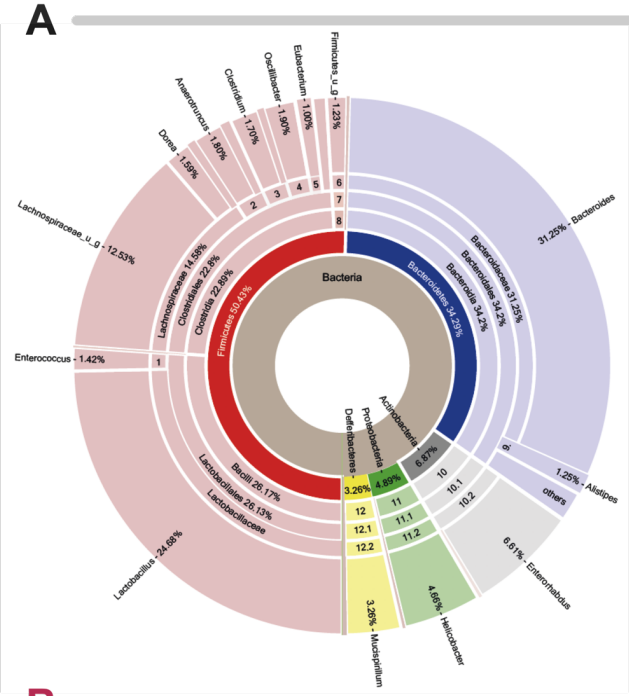

1	Enterococcaceae	1.42%	10	Coriobacteria.	6.81%
2	Ruminococcaceae	2.44%	11	Epsilonproteobacteria	4.66%
3	Clostridiaceae	2.08%	12	Defferibacters	3.26%
4	Oscillospiraceae	1.94%	10.1	Eggerthelaceae	6.78%
5	Eubacteriaceae	1.01%	10.2	Eggerthelaceae	6.78%
6	Firmicutes_u_f	1.23%	11.1	Campylobacterales	4.66%
7	Firmicutes_u_o	1.23%	11.2	Helicobacteraceae	4.66%
8	Firmicutes_u_c	1.23%	12.1	Defferibacterales	3.26%
9	Rikencellaceae	1.25%	12.2	Defferibacteraceae	3.26%

B CST-KO

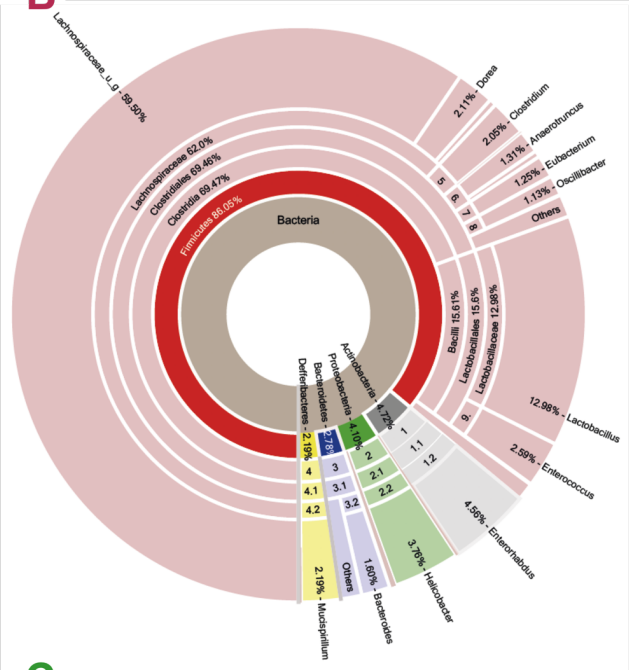

1	Coriobacteria	4.65%	4	Defferibacters	2.19%
1.1	Eggerthellales	4.63%	4.1	Defferibacterales	2.19%
1.2	Eggerthelaceae	0.06%	4.2	Defferibacteraceae	2.19%
2	Epsilonproteobacteria	3.76%	5	Clostridiaceae	2.06%
2.1	Campylobacterales	3.76%	6	Ruminococcaceae	1.67%
2.2	Helicobacteraceae	3.76%	7	Eubacteriaceae	1.28%
3	Bacteroidia	2.78%	8	Oscillospiraceae	1.16%
3.1	Bacteroidales	2.78%	9	Enterococcaceae	2.59%
3.2	Bacteroidaceae	1.60%			

C CgA-KO

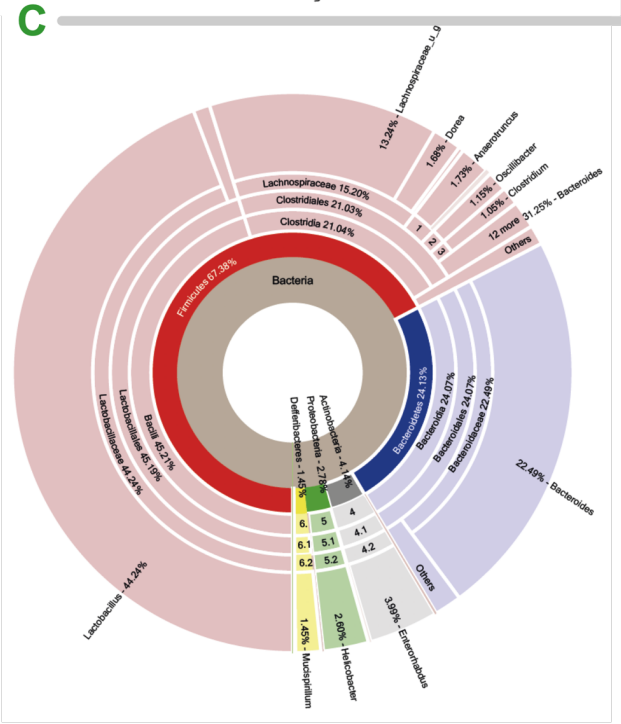

1	Ruminococcaceae	2.03%
2	Oscillospiraceae	1.16%
3	Clostridiaceae	0.06%
4	Coriobacteria	4.14%
4.1	Eggerthelaceae	4.09%
4.2	Eggerthelaceae	4.09%
5	Epsilonproteobacteria	2.06%
5.1	Campylobacterales	2.06%
5.2	Helicobacteraceae	2.06%
6	Defferibacters	1.45%
6.1	Defferibacterales	1.45%
6.2	Defferibacteraceae	1.45%

Fig. 7

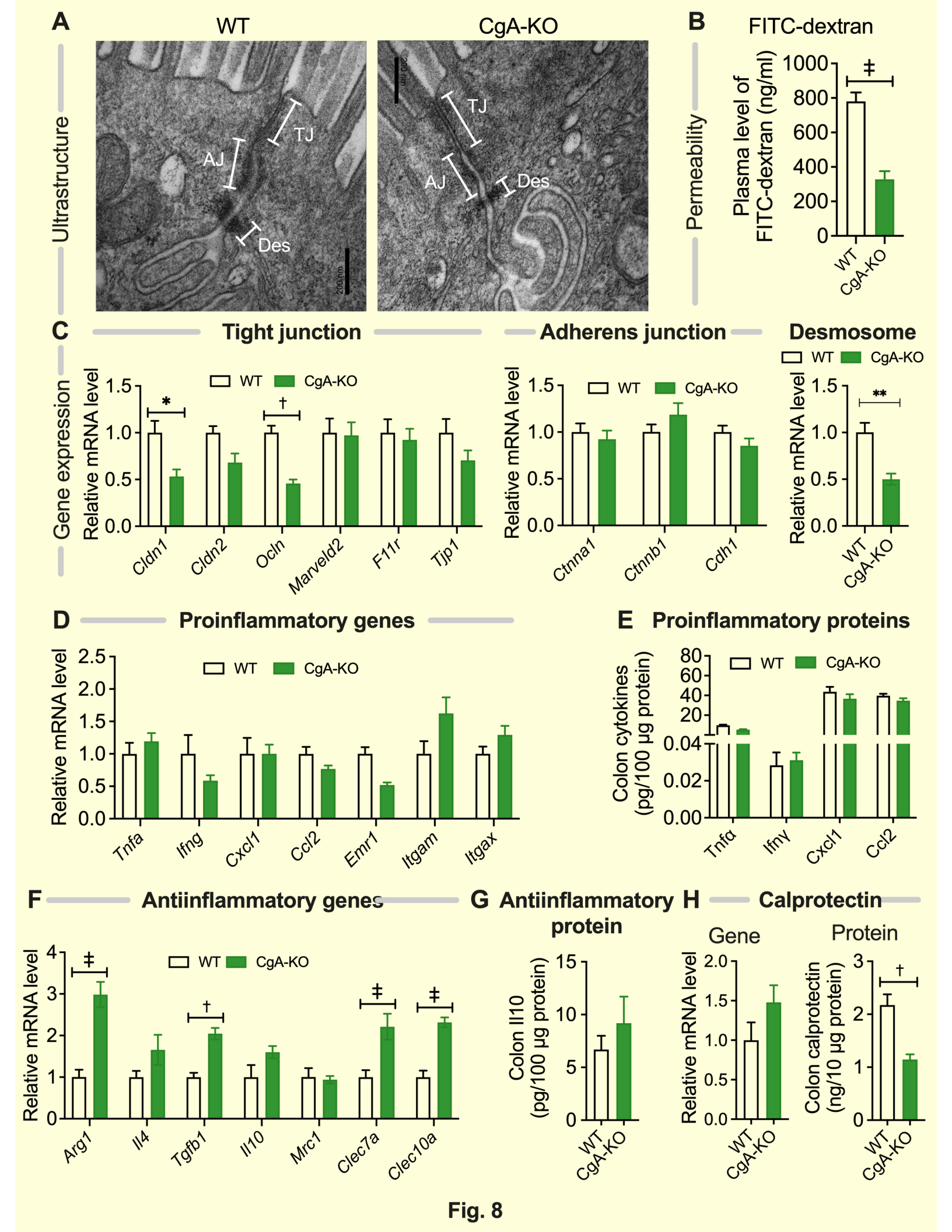
A
WT
CgA-KO
Ultrastructure
TJ
AJ
Des
200 nm
B
FITC-dextran
Permeability
Plasma level of FITC-dextran (ng/ml)
1000
800
600
400
200
0
‡
WT
CgA-KO
C
Tight junction
Adherens junction
Desmosome
Gene expression
Relative mRNA level
1.5
1.0
0.5
0.0
WT
CgA-KO
*
†
**
Cldn1
Cldn2
Ocln
Marveld2
F11r
Tjp1
Ctnna1
Ctnnb1
Cdh1
D
Proinflammatory genes
2.5
2.0
Tnfa
Ifng
Cxcl1
Ccl2
Emr1
Itgam
Itgax
E
Proinflammatory proteins
Colon cytokines (pg/100 µg protein)
80
60
40
20
0.04
0.02
0.00
Tnfα
Ifnγ
F
Antiinflammatory genes
4
3
2
1
0
‡
Arg1
Il4
Tgfb1
Il10
Mrc1
Clec7a
Clec10a
G
Antiinflammatory protein
Colon Il10 (pg/100 µg protein)
15
10
5
H
Calprotectin
Gene
Protein
Colon calprotectin (ng/10 µg protein)

Fig. 8

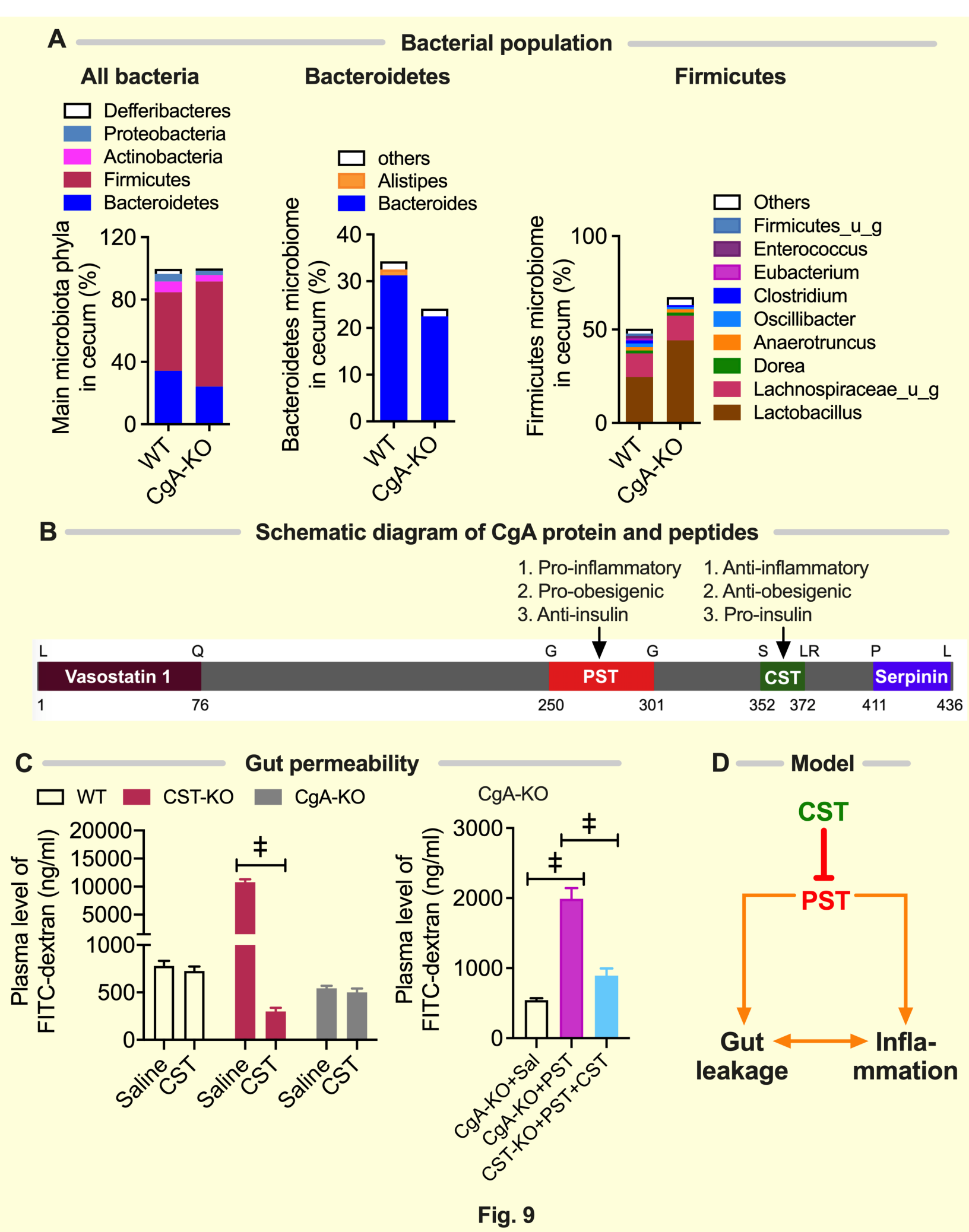
A
Bacterial population
All bacteria
Bacteroidetes
Firmicutes
Defferibacteres
Proteobacteria
Actinobacteria
Firmicutes
Bacteroidetes
Main microbiota phyla in cecum (%)
120
80
40
0
WT
CgA-KO
others
Alistipes
Bacteroides
Bacteroidetes microbiome in cecum (%)
40
30
20
10
0
WT
CgA-KO
Others
Firmicutes_u_g
Enterococcus
Eubacterium
Clostridium
Oscillibacter
Anaerotruncus
Dorea
Lachnospiraceae_u_g
Lactobacillus
Firmicutes microbiome in cecum (%)
100
50
0
WT
CgA-KO
B
Schematic diagram of CgA protein and peptides
1. Pro-inflammatory
2. Pro-obesigenic
3. Anti-insulin
1. Anti-inflammatory
2. Anti-obesigenic
3. Pro-insulin
L
Q
G
G
S
LR
P
L
Vasostatin 1
PST
CST
Serpinin
1
76
250
301
352
372
411
436
C
Gut permeability
WT
CST-KO
CgA-KO
Plasma level of FITC-dextran (ng/ml)
20000
15000
10000
5000
1000
500
0
‡
Saline
CST
Saline
CST
Saline
CST
CgA-KO
Plasma level of FITC-dextran (ng/ml)
3000
2000
1000
0
‡
‡
CgA-KO+Sal
CgA-KO+PST
CST-KO+PST+CST
D
Model
CST
PST
Gut leakage
Infla-mmation

Fig. 9